

General comment on the major revisions: For the major revisions of our discussion paper, we had to add two additional figures to the supplement of the paper (Fig. S12, S13). This was necessary to account for the details discussed in the answer to both reviews as demanded by the editor. Also we added two new chapters to the discussion part of the paper for the same reason. The chapter Sect. 4.3 “Key points to be considered for the application to real data” describes the benefits of our novel inversion approach together with different sources of signal noise and unknowns that have to be considered for the inversions of real measured data using our approach. The chapter Sect. 4.4: “Proof of concept for glacial data” contains preliminary results, showing the functionality of our approach for the inversion of glacial $\delta^{15}\text{N}$ data. Furthermore, we changed the abstract, the introduction and the conclusion in order to better explain the aim of the paper together with the functionality and benefits of our novel gas isotope inversion approach. With these changes the length of the manuscript text increased, yet we significantly decreased the number of figures.

The following replies to both reviewers are already published online.

The reply to the review of Anonymous Referee #2 can be found on pages 1-11, the reply to the review of Anonymous Referee #1 on pages 12-15.

Reply to reviewer 2:

We thank reviewer 2 for the detailed examination of the presented work. This allows us to clarify some issues potentially not emphasized enough within our discussion manuscript. Therefore we will use this opportunity to address major issues together with detailed answers to the key points mentioned by the reviewers. Reviewer comments are given in italic letters whereas our replies are given in normal letters.

Point (1):

The method assumes that the forward problem (converting surface temperature to $d15\text{N}$) is completely described by the firn model, and that all variations in $d15\text{N}$ can be linked 1-to-1 to past surface temperature. It is thus no surprise that they can reconstruct the original temperature very accurately, because they know the exact accumulation rates and physics of the forward model. Unfortunately, that is not at all true in the real world.

We are well aware of the fact that this assumption does not hold true. Due to uncertainties and simplifications in firn densification and gas diffusion physics, uncertainties in common firn models and measurement data our assumption is only an approximation of the real world as mentioned by the reviewer. Therefore, we will discuss several issues in this reply to reviewer 2. Nevertheless we used this assumption here to demonstrate the functionality of the automated fitting algorithm. Detailed uncertainty estimations for a “real world” scenario as demanded by the reviewer are behind the scope of this work and will follow for the reconstructions using measurement data ($\delta^{15}\text{N}$, $\delta^{40}\text{Ar}$, $\delta^{15}\text{N}_{\text{excess}}$) in next publications. Again, the aim of this work is to present the automated gas isotope fitting algorithm applied to synthetic Holocene $\delta^{15}\text{N}$ data and to study the uncertainties emerging from the algorithm itself. Furthermore the focal question in this study is: what is the minimum final mismatch in $\delta^{15}\text{N}$ for Holocene data we can reach and what does this mean for the final temperature mismatches. Studying and moreover answering these questions makes it mandatory to create well defined $\delta^{15}\text{N}$ targets and related temperature histories, as we did here. It is impossible to answer these important questions in detail without using synthetic data in a methodology study. The aim is to evaluate the accuracy and associated uncertainty of the inverse method itself to be able to apply this method in a future study to a real $\delta^{15}\text{N}$ dataset. Here, of course, the original driving temperature history will be unknown.

The $d15\text{N}$ is influenced by variations in convective zone thickness (the CZ is ignored here altogether), firn layering that influences the lock-in process, melt layers and wind crusts, etc. Real data (as opposed to the synthetic data used) further suffer from analytical noise in the laboratory. All these things will reduce the ability to reconstruct temperature from $d15\text{N}$. Furthermore, our understanding of firn densification is incomplete, with several physical models giving different results, microstructure effects not included in models, and hypothesized influences of dust softening. All these effects remain unaccounted for, which further reduces the ability to use $d15\text{N}$. The authors use identical firn physics in the forward and inverse models, which is an idealization that is untenable.

Regarding the convective zone (CZ): The presented fitting algorithm was used together with the two most frequently used firn models for temperature reconstructions based on stable isotopes of air, the Schwander et al. (1997) model which has no CZ build in (or assumes a constant CZ of 0 m) and the Goujon firn model (Goujon et al., 2003) (which assumes a constant convective zone over time, that can easily be set in the code). This

difference between the two firm models only changes the absolute temperature rather than the temperature anomalies as it was shown by other studies (e.g., Guillevic et al. (2013), fig. 3). In the presented work, we show the results using the model from Schwander et al. (1997), because the differences between the obtained solutions using the two models are negligible besides a constant temperate offset of about 2.3K. Also, noteworthy is that there is no firm model at the moment which uses a dynamically changing CZ. Indeed, this should be investigated but requires additional intense work. Additionally, the knowledge of the time evolution of CZ changes for the time periods of millennia to several hundreds of millennia (in frequency and magnitude) is too poor to estimate the influence of this quantity on the reconstruction.

In addition, the algorithm is able to fit $\delta^{15}\text{N}$, $\delta^{40}\text{Ar}$ and $\delta^{15}\text{N}_{\text{excess}}$ data as mentioned in the paper (e.g. in the abstract at line 17). In fig.1 we show unpublished data to clarify that the algorithm is usable for $\delta^{15}\text{N}_{\text{excess}}$ besides $\delta^{15}\text{N}$ data. Here the $\delta^{15}\text{N}_{\text{excess}}$ data from Kobashi et al. (2008) was used as the fitting target using the same approach. We reach a final mismatch (2σ) of 3.7 permeg, which is below the analytic measurement uncertainty of 5.0 to 9.8 permeg of the measurement data. We hope that this is convincing enough to show the functionality of our algorithm also for this quantity. The automated inversion of different gas isotope quantities ($\delta^{15}\text{N}$, $\delta^{40}\text{Ar}$, $\delta^{15}\text{N}_{\text{excess}}$) provides a unique opportunity to study the difference of the gained solutions for the different targets and to improve our knowledge about the uncertainties of gas isotope based temperature reconstructions using a single firm model. Because of the “perfect physics scenario” as mentioned above it is not necessary to show the synthetic $\delta^{40}\text{Ar}$ and $\delta^{15}\text{N}_{\text{excess}}$ fits here, because the gained solutions are the same. This will be different when using measurement data. Here, differences between the temperature solutions gained from the single targets ($\delta^{15}\text{N}$, $\delta^{40}\text{Ar}$, $\delta^{15}\text{N}_{\text{excess}}$) will become obvious due to several sources of signal noise. These differences will allow to quantify the uncertainties associated with processes mentioned by the reviewer.

Next, the presented algorithm is not dependent on the firm model, which leads to the implication that the algorithm can be coupled to different firm models describing firm physics in different ways. An automated reconstruction algorithm avoiding manual manipulation and leading to reproducible solutions makes it possible for the first time, to study and learn from the differences between the solutions. Differences that then can be assigned to different firm models and their shortcomings, resulting in more robust uncertainty estimates as was possible before. Thus, the algorithm provides the possibility to test firm models by fitting different targets and as mentioned before to learn from the differences between the solutions obtained by matching single targets. This is exactly the reason the algorithm was developed for.

Several studies have shown that on the cm-scale there is much variation in parameters like $d15\text{N}$ and CH_4 , reflecting a staggered trapping of gas bubbles within the firm-ice transition zone. See e.g. Etheridge et al. (1992), Rhodes et al. (2016), and Mitchell et al. (2015). This may be relevant as the sample size is typically smaller than the average layer thickness.

This point is not related to the scope this paper. Within the scope of paleoclimate reconstruction, the pertinent focus is more on how to extract signals from gas isotope data rather than how to represent potential sources of signal noise. Of course signal noise (such as firm heterogeneity) should be included in the uncertainty estimation, which is planned in a future study dealing with modelling (among others) real $\delta^{15}\text{N}$ data. However, we will try to account for this question here. We fully agree, for the reconstruction using measurement data, it is necessary to keep cm scale variability in mind. Our view on this point can be summarized as follows: During the analytical analyses of ice core air data it is common to measure replicates for given depths, from which the measurement uncertainties of the gas isotope data is calculated using pooled-standard-deviation (Hedges L. V., 1985). Often it is not possible to take real replicates (same depth) and instead the replicates are taken from nearby depths. So, the cm scale variability is to some degree already included in the measurement uncertainty, because each measurement point represents the average over a few centimetres of ice. This is especially the case for low accumulation sites or glacial ice samples for which the vertical length of a sample (e.g., 10-25 cm long for the glacial part of the NGRIP ice core, Kindler et al., 2014) covers the equivalent of 20-50 yrs of ice at approx. 35 kyrs b2k. Increasing the depth resolution of the samples would increase our knowledge of cm scale variability, for e.g. identifying anomalous layers that could have been rapidly isolated from the surface due to a high density layer (e.g., Rosen et al. (2014)). As this variability is likely due to heterogeneity in the density profile, this may not help to better reconstruct a meaningful temperature history, rather to observe the source of signal noise. To sum up: The cm scale variability, in many cases, is already incorporated in the analytical noise obtained from gas

isotope measurements, due to analytical techniques themselves. Assuming the measurement uncertainty as Gaussian distributed, it is very easy to incorporate this source of uncertainty in the inverse modelling approach. This will increase the uncertainty of the temperature according to Eq. (9) in our manuscript using the presented approach. The same equation can also be used for the calculation of the uncertainty in temperature related to measurement uncertainty in general.

To answer the pertinent question of how to better extract a meaningful temperature history from a noisy ice core record, an excellent – but costly – solution is of course to use multiple ice cores. The GISP2 ice core has actually the chance to have a “sister ice core” drilled only a few kilometres apart (the GRIP ice core) and combining $\delta^{15}\text{N}$ -based temperature reconstructed from both ice cores is likely one of the best ways to overcome potential cm scale variability. A comparison of ice cores that were drilled even closer might be even more advantageous.

Gas diffusion and trapping smooths out the $d15\text{N}$ signal, which provides a fundamental limit on the time resolution at which surface temperature is recorded and could potentially be reconstructed.

The duration of gas diffusion from the top of the diffusive column to the bottom where the air is closed off in bubbles is for Holocene conditions in Greenland approximately in the order of 10 yr (Schwander et al. 1997), whereas the data resolution of the synthetic targets was set to 20 yr to mimic the measurement data from Kobashi et al. (2008) with a mean data resolution of about 17 yr (see section 2.4: “Generating synthetic target data”). In the study of Kindler et al. (2014) it was shown that a Glacial Greenland lock-in depth leads to a damping of the $\delta^{15}\text{N}$ signal of about 30% for a 10 K temperature rise in 20 yr. We further assume that the smoothing according to the lock-in process is negligible for Greenland Holocene conditions according to the much smaller amplitude signals and shallower lock-in depth for Holocene conditions.

From the above it is clear to me that the precision that the authors state for their method is a meaningless number, that teaches us nothing about how well $d15\text{N}$ can reconstruct temperature. A more interesting approach would be to include these fundamental uncertainties in a stochastic way, and see how well the method works under realistic settings. The synthetic data could e.g. be generated with a different firn physics description, and should be subject to CZ fluctuations, LIZ thickness variations and analytical noise.

This is obviously a misunderstanding. Indeed we did not mention that the mismatch in $\delta^{15}\text{N}$ and the therefrom calculated temperature range would correspond to an uncertainty of temperature reconstructions. This range is only the uncertainty part that directly relates to the inversion model approach and does not include any other uncertainties that exist. In the “perfect world” scenario it should be theoretically possible to reach a final mismatch of zero for $\delta^{15}\text{N}$ as well as for temperature. The reason why this was not reached in our study is related to the memory effects in the ice sheet model which leads to a rising computational effort for reaching very low mismatches. An improvement of one section of the time series will be paid by degradation in another part. To circumvent the computational demand we developed the correction step (step 4, section 2.4.4), which accounted for this memory effects. This means that in finite time there has to be a limit the algorithm can reach, which is exactly characterized by the final mismatches presented here.

Additionally, in the perspective of making a complete uncertainty budget for a temperature history reconstructed based on $\delta^{15}\text{N}$ data (again, as will be done in a future publication), this uncertainty value for the inverse modelling method, being not zero, cannot be neglected and should therefore be taken into account.

Point (2):

There are 2 fundamental inputs into the model, namely temperature and accumulation rate. The authors assume the latter is known with zero uncertainty (both in values and age model). This is a very unrealistic assumption. Even if the layer-count were perfect (which it is not), correcting for ice thinning has a fundamental uncertainty. Especially in the early Holocene, this can easily exceed 10%. As the method fits the $d15\text{N}$ data, all accumulation errors are mapped into the temperature reconstruction. This is not accounted for...As an aside, the authors convert the accumulation record from Cuffey et al. onto the GICC05 scale, which makes it internally inconsistent because the accumulation rate is the derivative of the age scale, so changing the age scale should change the accumulation values. Since the method is sensitive to the decadal-scale accumulation variability, it may be insufficient to use this crude approach.

Answer for the point on the conversion of the Cuffey accumulation record to the GICC05 time scale: We think this comment arose from a lack of details given in the paper. Therefore we describe in the following in more detail the procedure we used to produce the finally used accumulation rate data for our modelling work. The original accumulation rate for the GISP2 ice core is the one published in Cuffey and Clow (1997), produced using an ice flow model adapted to the GISP2 location. The accumulation rate used to feed the ice flow model was optimised in order to match the time scale from Meese et al. (1994) for the Holocene, based on annual layer counting. Seierstad et al. (2014) transferred the GISP2 chronology to the GICC05 reference timeframe using multiple match points to the NGRIP and GRIP ice cores, both already on GICC05. We used these match points and modified the GISP2 duration in between match points linearly in order for the considered interval to match exactly the GICC05 duration. This way, the detailed GISP2 annual layer counting information is kept, but is only stretched/compressed in time. This was done for all intervals in between two match points. The accumulation data were then re-calculated accordingly, as obviously (as stated by the reviewer) this is needed in order to keep the same total amount of ice accumulated at the GISP2 site. Actually, to obtain an even better consistency, the best would be to re-run the Cuffey and Clow ice sheet model, using the GICC05 timescale as target timescale, and use the resulting accumulation rate data (but this is beyond the scope of this study).

Furthermore, as we have shown in the paper in section 2.4 “Accumulation rate input”, the accumulation rate variability has a minor impact compared to the temperature on the variability of the $\delta^{15}\text{N}$ data in the Holocene (see also fig.A02). The influence of the quantities, accumulation rate or temperature, on the temperature reconstruction is not equal, the accumulation rate variability during the Holocene explains about 12 to 30% of the $\delta^{15}\text{N}$ variability. 30% corresponds to the 8.2 kyr event and 12% for the mean of the whole Holocene period including the 8.2 kyr event. Hence the influence of accumulation changes is generally below 10% during the Holocene. If the accumulation is assumed to be completely correct then the missing part will be assigned to temperature variations. Also in section 2.3.1 we show that the polynomial degree in temperature is more important than for the accumulation for the calculation of a polynomial transfer function (see line 3-6 at page 5 and fig.S02). Nevertheless for the fitting of the Holocene measurement data we will use all three accumulation rate scenarios as shown in fig.S01. The difference in the reconstructed temperature arising from the differences of these three scenarios will be used for the uncertainty calculation as well and is most likely higher than the uncertainty arising from the conversion of the accumulation rate data to the GICC05 timescale.

Point (3):

The authors have no way of validating that their Delta-age is correct, which is critical to constrain the timing of climate change. In all $d^{15}\text{N}$ modeling studies I'm aware of, the use of $d^{18}\text{O}$ as a temperature template ensures that Delta-age is correct. In particular during abrupt events, the timing of gas and ice signals gives you Delta-age. This information is lost in their method, which is completely independent of $d^{18}\text{O}$. If the modeled D_{age} is off by 50 years (which is easy to do in Greenland, particularly during the glacial), the timing of the temperature solution is also off by 50 years. It would be interesting to run their algorithm on data from the last deglaciation, and see whether it reproduces the timing of abrupt change as seen in $d^{18}\text{O}$. Because Deltaage is underconstrained, the timing of all reconstructed high-frequency temperature variations is uncertain.

We thank the reviewer for mentioning that point, since we have not explicitly discussed the behaviour of the Δ_{age} agreement in the paper and we will catch up on this. The Δ_{age} adjustment in the Holocene case is related to the smooth temperature solution calculated by the Monte Carlo part of the algorithm. If a smooth temperature solution is found which creates a robust long term signal in $\delta^{15}\text{N}$ the gas age - ice age difference from that model output is used to calculate the high frequency information and to find the right timing for adding the high frequency signal to the smooth temperature solution as it was explained in section 2.4.2 (page 9, lines 11-13) and section 2.4.3 (page 9, lines 18-23). As the measurement target data is set on the ice age scale (like all gas isotope data after measurement) and the accumulation rate is known, the high frequency temperature signal has to have the right timing when the final calculated $\delta^{15}\text{N}$ signal matches the target (or measurement) data. Table 1 contains the final mismatches (2σ) in Δ_{age} for all scenarios and shows very well that with a known accumulation rate and firn physics it is possible to fit the Δ_{age} history in the Holocene with mean uncertainties better than 2 yr. This table together with a similar statement will be added to the paper in the results section. Figure 2 shows the time series of the mismatches in Δ_{age} for all scenarios and is used to clarify the functionality of the algorithm itself.

More interesting for the reviewer is probably the “real world” scenario. Due to the large uncertainties in measured or modelled Δ age it is a challenging task to validate the correctness of the Δ age regime anyway. But to give an idea to that issue we show here ongoing work. Figure 3 shows the comparison of the Δ age regime modelled using our algorithm together with the GISP2 $\delta^{15}\text{N}$ data from Kobashi et al. (2008) and the Δ age regime published with the GICC05 GISP2 gas age scale from Seierstad et al. (2014) and Rasmussen et al. (2014). Besides a nearly constant offset of about 20 yr in the early Holocene the agreement is amazing with a standard deviation (2σ) of the mismatches of 7.8 yr over the whole time series and 3.5 yr for the last 8.2 kyr.

For Glacial conditions the task of reconstructing the temperature (with the right frequency and magnitude) without $\delta^{18}\text{O}_{\text{ice}}$ information is much more challenging as mentioned by the reviewer due to the highly variable gas age - ice age differences between stadial and interstadial conditions. Here the Δ age can vary several hundreds of years. Also the accumulation rate data is more uncertain than in the Holocene. To prove that the presented fitting algorithm also works for Glacial conditions we inverted the $\delta^{15}\text{N}$ data measured for the NGRIP ice core by Kindler et al. (2014) for two Dansgaard-Oeschger events, namely DO6 and DO7. Since the magnitudes of those events are higher and the signals are smoother than in the Holocene we only had to use the Monte Carlo type input generator (section 2.4.2) for changing the temperature inputs. To compare our results to the $\delta^{18}\text{O}_{\text{ice}}$ based manually calibration method from Kindler et al. (2014) we used the ss09sea06bm time scale (NGRIP members (2004), Johnsen et al. (2001)) as it was done in the Kindler et al. publication. For the model spin-up we use the accumulation rate and temperature data from Kindler et al. (2014) for the time span 36.2 to 60 kyr. The reconstruction window (containing DO6 and DO7) was set to 32 to 36.2 kyr. As the first guess (starting point) of the reconstruction we used the accumulation rate data for NGRIP from the ss09sea06bm time scale together with a constant temperature of about $-49\text{ }^\circ\text{C}$ for this time window. As minimization criterion D for the reconstruction we simply use the sum of the mean squared errors (wRMSE) of the $\delta^{15}\text{N}$ and Δ age mismatches weighted with their uncertainties according to the following equation instead of the mean $\delta^{15}\text{N}$ misfit alone as used for the Holocene.

$$D = \sqrt{\text{wRMSE}(\delta^{15}\text{N})} + \sqrt{\text{wRMSE}(\Delta\text{age})} \quad (1)$$

$$= \sqrt{\frac{1}{N} \sum_i \left[\frac{\delta^{15}\text{N}_{\text{meas},i} - \delta^{15}\text{N}_{\text{mod},i}}{\varepsilon_{\delta^{15}\text{N},i}} \right]^2} + \sqrt{\frac{1}{M} \sum_j \left[\frac{\Delta\text{age}_{\text{meas},j} - \Delta\text{age}_{\text{mod},j}}{\varepsilon_{\Delta\text{age},j}} \right]^2}$$

Here $\varepsilon_{\delta^{15}\text{N},i}$ and $\varepsilon_{\Delta\text{age},j}$ are the uncertainties in $\delta^{15}\text{N}$ and Δ age for the measured values i or j (Δ age match points: Guillevic, M. (2013), p.65, Tab. 3.2) and N, M the number of measurement values. We set $\varepsilon_{\delta^{15}\text{N},i} = 20$ permeg for all i (Kindler et al. 2014) and $\varepsilon_{\Delta\text{age},j} = 50$ yr for all j . The values of 50 yr for the Δ age uncertainties were chosen according to reach the same mean relative errors for both terms. The relative uncertainties in Δ age can easily reach up to 50% and more in the Glacial using the ss09sea06bm time scale which results in a domination of the $\delta^{15}\text{N}$ misfits over the Δ age misfits (10-20% when using GICC05 time scale, pers. communication M. Guillevic). Because of that issue we had to set the Δ age uncertainties to 50 yr to make both terms equally important for the fitting algorithm. To sum up: The temperature variations were exactly done in the same way as described in section 2.4.2 within the paper without any further adjustments. We only had to add one target more (Δ age) to the minimization criterion to account for a second unknown, i.e. the also uncertain accumulation rates. In fig.4 we show preliminary results. The $\delta^{15}\text{N}$ and Δ age fitting (a,b) and the resulting gained temperature and accumulation rate solutions (c,d) using the presented algorithm are completely independent from $\delta^{18}\text{O}$ which provides a great opportunity to evaluate the $\delta^{18}\text{O}$ based reconstruction. In this study the algorithm was used in three steps (MCS0, MCS1, MCS FIN). First, starting with the first guess (constant temperature), the temperature was changed as explained before. The accumulation rate was changed parallel to the temperature allowing a random offset shift (up and down) together with a stretching or compressing (in y direction) of the accumulation rate signal over the whole time window (32 to 36.2 kyr). This first step leads to the “Monte Carlo Solution 0” (MCS0) which provides a first approximation and is the base for the next step. For the next step, we fixed the accumulation rate and let the algorithm only changes the temperature to improve the $\delta^{15}\text{N}$ fit (MSC1). Finally, we allow the algorithm to change the temperature together with the accumulation rate using the Monte Carlo type input generator for both quantities. This also allows the change of the shape of the accumulation rate data. This final step can be seen as a fine tuning of the gained solutions from the steps before. The reached

mismatches in $\delta^{15}\text{N}$ and Δage of all steps are at least of the same quality or better than the $\delta^{18}\text{O}$ based manual method from Kindler et al. (2014) (see Tab.2). The gained temperature solutions show a very good agreement in timing and magnitude compared to the reconstruction of Kindler et al. (2014). Also the accumulation rate solutions show that the accumulation has to be reduced significantly compared to the ss09sea06bm data to allow a high quality fit of the $\delta^{15}\text{N}$ and Δage target data, a result highly similar to Kindler et al. (2014) and Guillevic et al. (2013). Regarding the mismatches in $\delta^{15}\text{N}$ and Δage of the final MCS FIN solution show a 15% smaller misfit in $\delta^{15}\text{N}$ (2σ) and an about 31% smaller misfit for Δage (2σ). Keeping in mind that the used approach is completely independent from $\delta^{18}\text{O}$ should clarify the functionality and quality of the presented gas isotope fitting approach also for Glacial reconstructions.

Point (4):

I am surprised the authors don't even attempt to invert the existing GISP2 data (which are even plotted). This seems like a missed opportunity; especially given that it would allow comparison to existing reconstructions to estimate the accuracy of the method.

We understand the surprise of the reviewer of the missing application on existing data but the focus on this paper is indeed the inversion model, its mathematics as well as a proper analysis on the capabilities of the algorithm itself based on a synthetic data set. Yet, we will provide a limited projection on future publications hereafter. However, we underline once more that the accuracy of the inverse modelling algorithm can only be estimated using a synthetic dataset, as shown in our paper. The GISP2 data for $\delta^{15}\text{N}$, $\delta^{40}\text{Ar}$ and $\delta^{15}\text{N}_{\text{excess}}$ are already inverted using the presented algorithm and will be presented in a following publication, since there are a couple of items to be addressed in detail which would overload the scope of the present methodological manuscript. But we want to discuss the algorithm itself to examine what are the possibilities and the limits of the presented fitting method in a well-known modelling frame work. The main focus of the present manuscript is to present the algorithm in a single publication rather than in the supplementary to bring the attention on the functionality and fundamental ideas of the algorithm rather than on the gained solutions. We think that is important to give the interested reader the chance to understand the basic concepts behind the algorithm and to show the functionality on a well-known example (here synthetic $\delta^{15}\text{N}$). We hope that we can simplify gas isotope based reconstructions for a broad spectrum of researchers using our or maybe a related approach later on. As we have shown, the approach works for all relevant gas isotope quantities ($\delta^{15}\text{N}$, $\delta^{40}\text{Ar}$, $\delta^{15}\text{N}_{\text{excess}}$) and for Holocene as well as Glacial data. The approach is a completely new method which enables the automatized fitting of gas isotope data without manual tuning of parameters minimizing the “subjective” impact of a single researcher. All together we are sure that this paper is the best way to present our new elegant fitting method in the framework we have chosen.

Point (5):

The paper is overly long. I recommend section 2.3 be removed entirely, and other sections be shortened considerably. There are also 32 (!) figures in the manuscript, which is too many. Dividing the figures into main, appendix and supplement figures is annoying, as it requires a lot of going back and forth.

We agree that the paper is long and that the amount of figures is possibly too much. As already stated, we tried to explain and discuss the algorithm in every detail to clarify the functionality of all parts of the fitting method. Our aim was also to present this new method in a totally transparent manner. To shorten the paper we will remove section 2.3 as suggested by the reviewer. This section was thought as a motivation for the presented fitting algorithm. We agree that it is not necessary for the paper itself. Also, we will reduce the numbers of figures by removing the following figures:

Main part: fig01, fig02, fig03

Supplementary: fig.S02 to fig.S16

Next we will shift all the appendix figures in a new supplementary. This means that we will have now 4 figures in the manuscript and 11 figures in the supplementary. As we want to keep the paper understandable a further reduction of figures and pages is not possible.

Detailed comments:

Page 1 Line 26: Give references for Holocene temperature reconstructions (there are many!).

Since we developed a novel algorithm for ice core based temperature reconstructions and explained the functionality based on synthetic data of Holocene like behaviour, we gave references to other ice core based reconstruction methods. (borehole inversion, page 1 line 6ff; calibration of water isotopes from the ice core water samples, page 1 line 9ff; $\delta^{15}\text{N}$, $\delta^{40}\text{Ar}$, $\delta^{15}\text{N}_{\text{excess}}$ based methods, page 1 line 14ff). Because no reconstruction for measurement data is shown here, we think it is not necessary to refer for other (or non-ice-core-based) reconstructions.

Page 3 Eq. (1): what about the convective zone? You should correct for that Eq. (2): The surface temperature should really be the temperature at the bottom of the convective zone where diffusion starts to dominate. This may smooth out some of the abrupt decadal-scale temperature variations.

The Schwander model does not use a convective zone at this stage but such a CZ could be implemented in the calculation of $\delta^{15}\text{N}_{\text{grav}}$, by subtracting the gravitational signal formed over the length of the CZ. Has the reviewer examples of a convective zone deep enough to smooth out decadal scale signals except “Megadune” sites (Severinghaus et al., 2010)? We are a bit surprised with this sentence, as for example J. Severinghaus, using measurements done at South Pole, showed that the seasonal signal in gas diffusion already affects the first 10 to 12 m of firn (Severinghaus, 1998) pointing to a shallow or even non-existing CZ. Furthermore, we have to remember that we are discussing the rather stable Holocene period in Greenland for which no low accumulation and strong katabatic wind situations are to be expected minimizing the effect of deep CZ. For a CZ to have an effect as strong as to smooth out decadal scale variation, its deepness would need to be of several dozens of meters, which is highly unrealistic even for Glacial Summit conditions. Contrary the process definitely affecting the damping of the signal is gas diffusion occurring in the firn, producing i) an increase in the mean gas age of the gas at the LID and ii) a damping of the signal whose amplitude is positively correlated with the LID (see for example, Buizert et al. (2012), Fig. 7; Buizert et al. (2013), Fig. 2; and Kindler et al. (2014), Fig. 2).

Line 17: Martinerie et al. (1994) gives the depth of the bubble close-off, whereas $d_{15\text{N}}$ is set at the lock-in depth instead. The LID is shallower than the COD. Is this difference accounted for, and how?

This is explained in details in the description of the Schwander firn model (Schwander, 1997). We did not report details in this paper because we thought this model is i) already quite well known and ii) well described in its original paper. However we report this information here: Indeed it is well known that the LID is shallower than the COD, due to the presence of a non-diffusive zone. Originally the COD is defined by a density threshold, calculated as a function of temperature (Marterie et al., 1994). In the Schwander model, to account for the presence of the non-diffusive zone, this COD definition is modified by subtracting 14 kg/m³ to the COD density definition, in order to match the observed depth where gas diffusion stops. This offset was optimised using firn data from Summit (GRIP) collected in the 90', Greenland, and we therefore believe this definition is highly appropriate for the GISP2 site over the Holocene.

Page 4 Section 2.2: what are the model parameters? What are the time and spatial step? How deep does the domain extend? What geothermal heat flux is used, etc.

The model parameters are described in detail in Schwander et al. (1997).

Section 2.3: I recommend this is removed completely. I don't see the point, especially the dynamic case which we know doesn't behave linearly due to memory effects.

To shorten the paper we will remove this section as suggested by the reviewer. This section was thought as a motivation for the presented fitting algorithm. We agree that it is not necessary for the paper itself.

Page 6 Line 13: Not too robust. It'd be easy to have a 10% uncertainty in the thinning function.

We reformulate these sentences from:

“Except for these technical adjustments, the accumulation rate input data remains unmodified, assuming high reliability of this data during the Holocene. This is due to the fact that the data was gained by annual layer counting, and the use of a thinning model which should be rather robust for the first 1500 m of the 3000 m ice core (Cuffey and Clow, 1997).”

The new text now reads:

“Except for these technical adjustments, the accumulation rate input data remains unmodified, assuming high reliability of this data during the Holocene. The data was gained by annual layer counting, and the use of a thinning model which should lead to maximum relative uncertainty of 10% for the first 1500 m of the 3000 m ice core (Cuffey and Clow, 1997).”

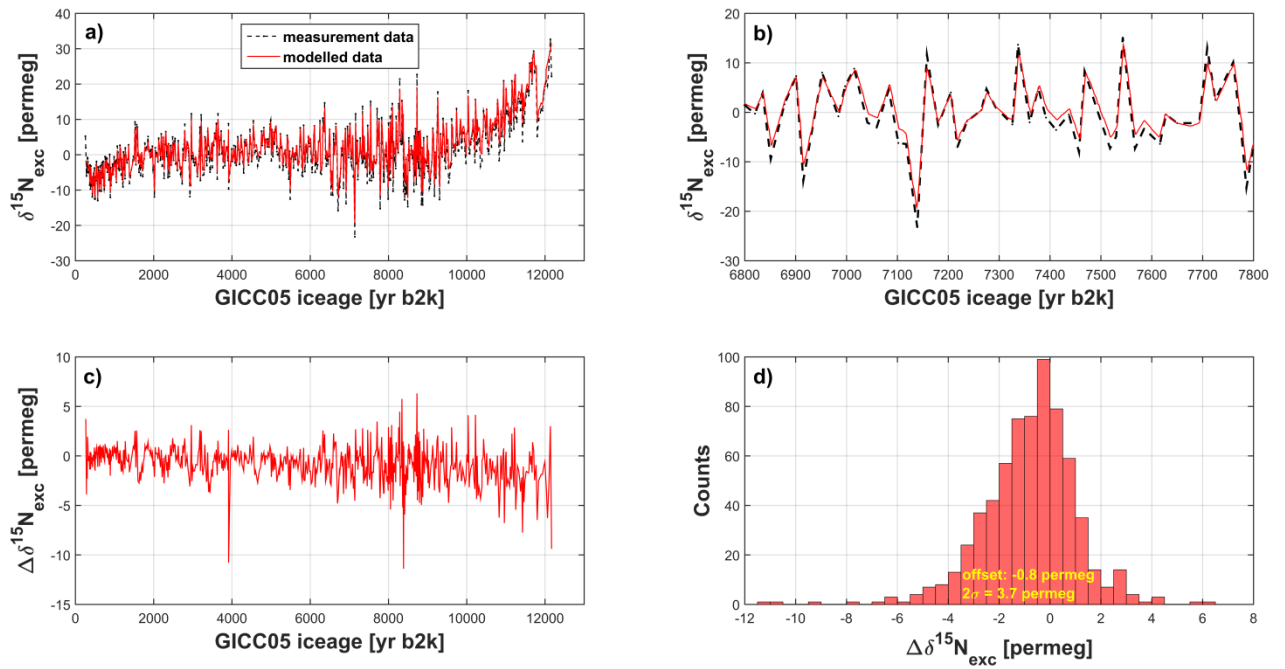


Fig.1: Fitting of GISP2 $\delta^{15}\text{N}_{\text{excess}}$ data (measurement data from Kobashi et al. 2008): a) measured versus modelled $\delta^{15}\text{N}_{\text{excess}}$ time series; b) zoom-in for a randomly chosen 1000 yr interval; c) time series of final mismatches $\Delta\delta^{15}\text{N}_{\text{excess}}$ for the measured minus the modelled $\delta^{15}\text{N}_{\text{excess}}$ data; d) histogram for the same quantity as in c) with values for the final mismatch (2σ) and offset;

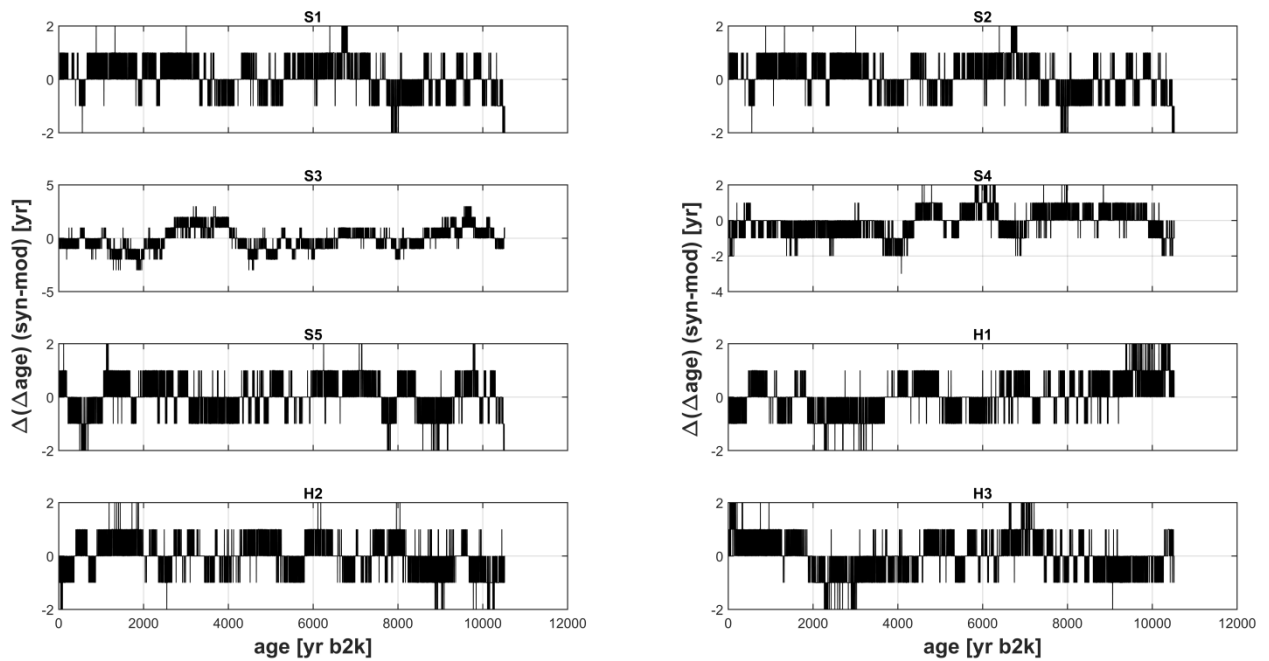


Fig.2: Comparison of the mismatches in Δage between the synthetic target and modelled data for all scenarios showing excellent agreement in Δage . All fits leads to a mean mismatch $\Delta(\Delta\text{age})$ in Δage better than 2yr (2σ).

Scenario:	$2\sigma \Delta(\Delta\text{age})$ [yr]	Scenario:	$2\sigma \Delta(\Delta\text{age})$ [yr]
S1	1.14	S5	1.24
S2	1.60	H1	1.23
S3	1.98	H2	1.18
S4	1.41	H3	1.30

Tab.1: Final mismatches (2σ) of Δage for all scenarios.

Solution	D	Mismatch $\delta^{15}\text{N}$ (2σ) [permeg]	Mean mismatch $\delta^{15}\text{N}^*$ [permeg]	Mismatch Δage (2σ) [yr]	Mean mismatch Δage^* [yr]
Kindler 2014	3.6	44.5	17.9	256	101
first guess	7.8	128.7	63.8	328	138
MCS0	3.1	50.0	19.3	199	82
MCS1	2.9	44.3	17.6	200	84
MCS FIN	2.6	37.8	15.6	175	63

Tab.2: Prove of concept for Glacial reconstruction; *The mean mismatches for $\delta^{15}\text{N}$ and Δage were calculated according to Eq. (7) in the paper.

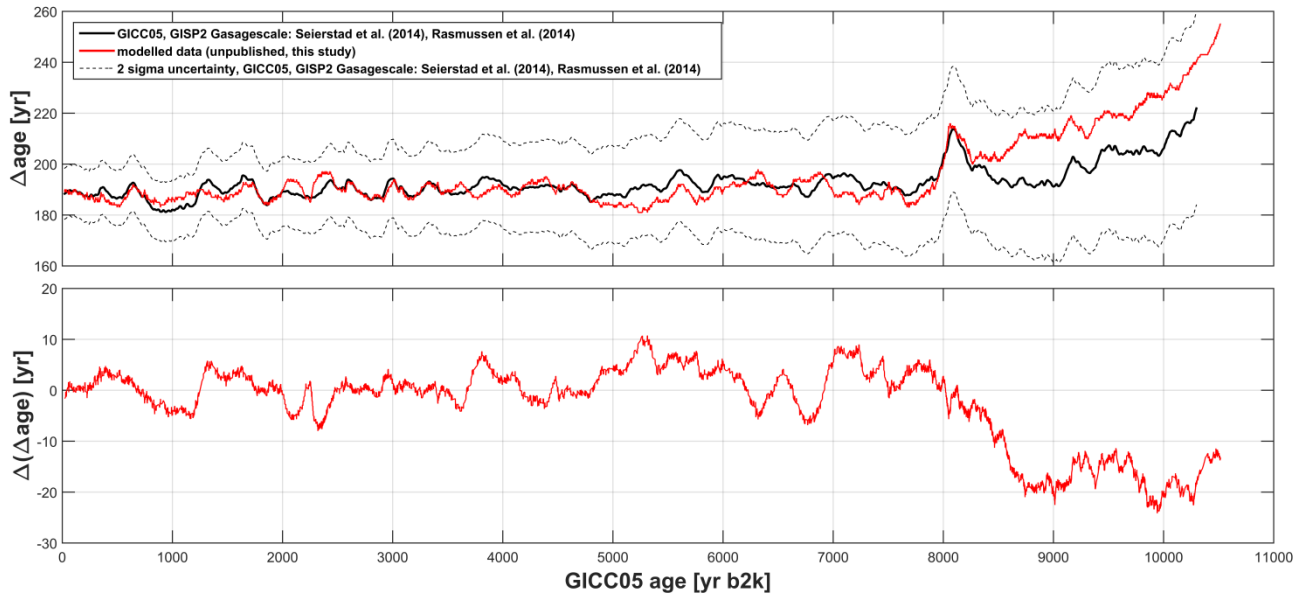


Fig.3: Top plot: Comparison of the modelled Δage (red, unpublished/this study) using the presented approach together with the Schwander model and $\delta^{15}\text{N}$ target data (Kobashi et. all 2008) with the Δage time series for GICC05 GISP2 gasagescale (black curve) from Seierstad et al. (2014), Rasmussen et al. (2014) and related 2σ uncertainty (dotted line). Bottom plot: Time series of the mismatches $\Delta(\Delta\text{age})$ in Δage .

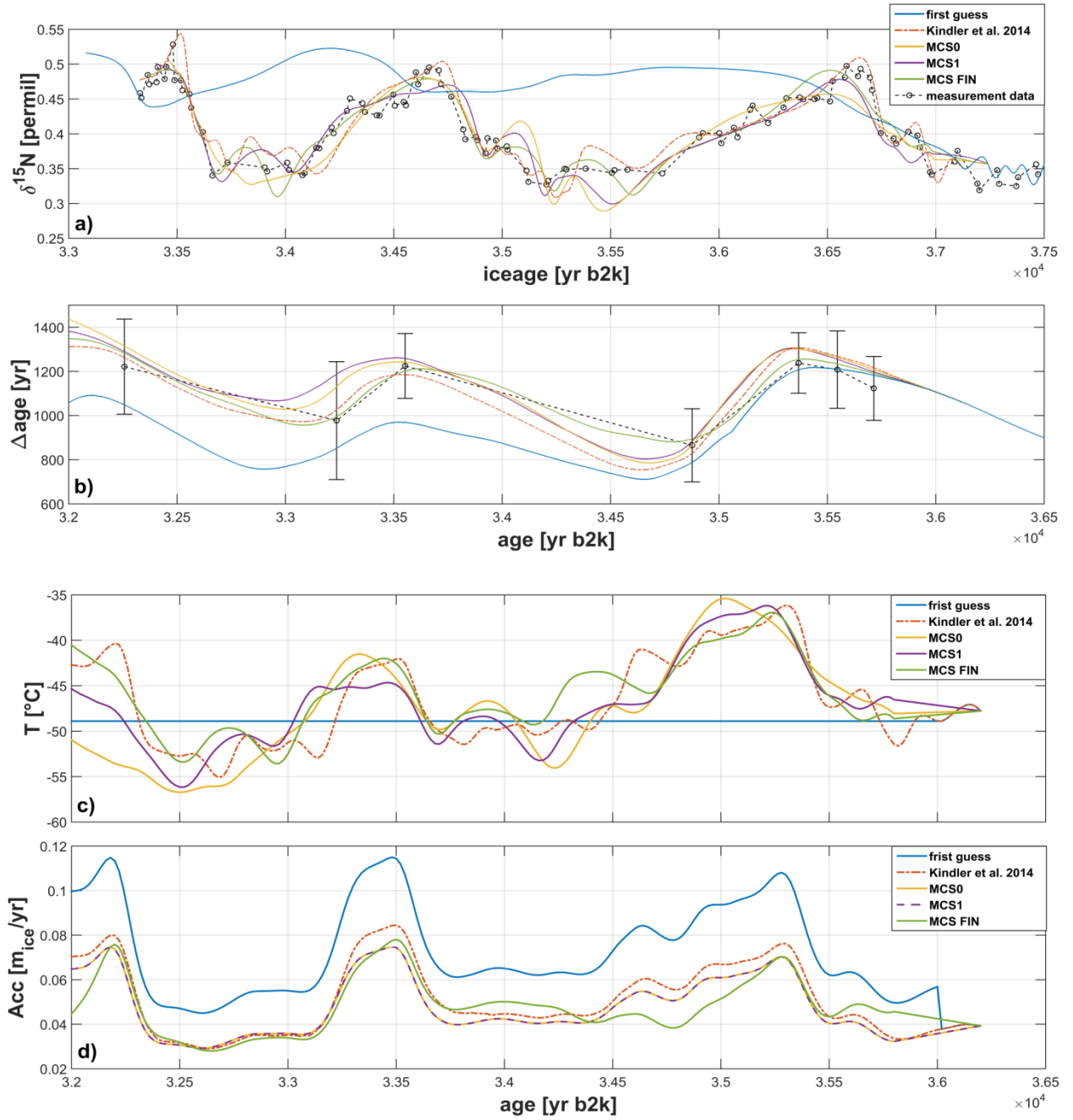


Fig.4: Prove of concept for Glacial reconstructions (NGRIP DO6 and DO7): a) $\delta^{15}\text{N}$ target plot: $\delta^{15}\text{N}$ model output for the first guess input (blue line), Kindler et al. (2014) fit (orange dotted line), Monte Carlo solution 0 (yellow line, unpublished data), Monte Carlo solution 1 (purple line, unpublished data), final Monte Carlo solution (green line, unpublished data), $\delta^{15}\text{N}$ measurement target (black dotted line, measurement points are black cycles, data from Kindler et al. (2014)); b) Δage target plot: Δage model output for the first guess input (blue line), Kindler et al. (2014) fit (orange dotted line), Monte Carlo solution 0 (yellow line, unpublished data), Monte Carlo solution 1 (purple line, unpublished data), final Monte Carlo solution (green line, unpublished data), Δage measurement target (black dotted line, measurement points are black cycles, data from Guillevic (2013)); c) temperature solution plot: first guess input (blue line), Kindler et al. (2014) solution (orange dotted line), Monte Carlo solution 0 (yellow line, unpublished data), Monte Carlo solution 1 (purple line, unpublished data), final Monte Carlo solution (green line, unpublished data); d) accumulation rate solution plot: first guess input (blue line), Kindler et al. (2014) solution (orange dotted line), Monte Carlo solution 0 (yellow line, unpublished data), Monte Carlo solution 1 (purple line, unpublished data), final Monte Carlo solution (green line, unpublished data);

Reply to reviewer 1:

General Comment on reviewer 1:

It was very difficult to find in the comment from reviewer 1 a scientific and/or technical discussion on the scientific questions the presented work is dealing with. Therefore it is challenging to find an appropriate way to answer the remarks and comments of this review. However, we will try to address the key issues and will give an adequate answer in the best possible manner.

This work describes a technical and mathematical variation on previously published work by Kobashi et al. (2010; 2011; 2012).

That is not true at all, which makes us wonder if the reviewer read in detail our submitted article. The presented approach is completely different to the mentioned work of Kobashi et al.. The calculation of temperature gradients from $\delta^{15}\text{N}_{\text{excess}}$ data used for a temporal integration using the Goujon model as it was done by Kobashi differs from our approach significantly. Our approach calculates in a first step a long term temperature signal and the isotope target, which is superimposed by a high frequency signal in a next step. Finally we created a correction method for dealing with remaining misfits (permeg level) due to memory effects. Besides the methodology view, we will list 6 major differences between both methods:

- (1) Our approach allows the automated high quality fitting (or inversion) of $\delta^{15}\text{N}$ or $\delta^{40}\text{Ar}$ or $\delta^{15}\text{N}_{\text{excess}}$ data as single targets (as it was mentioned in the paper and shown in the answer to reviewer 2) and provides consequently the opportunity to compare the solution of one target against the others. The method from Kobashi et al. uses all isotope quantities together, eliminating the possibility to compare the reconstruction obtained from one quantity using the other ones.
- (2) Our approach is applicable to Holocene as well as Glacial data (as it was mentioned in the paper and shown in the answer to reviewer 2), whereas the approach of Kobashi et al. was only designed and tested for Holocene reconstructions.
- (3) Our approach allows a parallel adjustment of the accumulation rate input data (if it is necessary) (shown in the answer to reviewer 2 for Glacial data).
- (4) Our approach uses a well-defined minimization criterion which provides the possibility to adapt it to a variety of target combinations (e.g. $\delta^{15}\text{N}$ and Δage for Glacial reconstructions).
- (5) Our approach is not dependent on the choice of a first guess for the reconstruction. A worse choice of this quantity will only elongate the computational time of the “Monte Carlo type input generator” step. This was shown since we used the same first guess (a constant temperature) for all different synthetic data scenarios.
- (6) Our approach splits the reconstructed temperature and isotope signals in a long term and a high frequency signal (for Holocene), which provides additional information and bases for further research questions and uncertainty calculations.

Kobashi et al. innovated by creating a novel hybrid firn densification-thermal diffusion model, much the same as is done here.

To our knowledge, Kobashi et al. used for their reconstruction the already published model from Goujon et al. (2003). The Goujon model is indeed a firn densification model, coupled to an ice sheet flow model also calculating heat transfer from surface to bedrock. The Goujon model does not have a module to automatically optimise the temperature and accumulation scenario needed for the inversion. We agree to this comment in the sense that Kobashi et al. indeed innovated a novel technique to create an input temperature scenario to feed the Goujon model, using firn temperature gradients extracted from $\delta^{15}\text{N}_{\text{excess}}$. We also agree that our approach, similar to the method from Kobashi, needs a firn densification and heat diffusion model to provide the physical basis for the inversion of $\delta^{15}\text{N}$ data. Nevertheless both methods differ significantly from each other as discussed before. Also both methods were created independently.

The scientific advance represented by this work is useful but is very incremental, almost to the point of not standing alone as a publishable scientific paper. It is not clear to me that this work suffices as a "Least Publishable Unit", and reads more like an Appendix to a publication.

We think that this is a very subjective opinion which is not underpinned by any scientific argument. We created a completely automated algorithm which is able to provide high quality fits for all relevant gas isotope quantities and works as well for Holocene as Glacial conditions. Furthermore the algorithm is not firn model dependent as it was coupled on two state of the art firn models, leading to comparable results. We also refer to the answer on reviewer 2 for point 1, explaining the achievements of this method in detail. Moreover, there are many examples of models presented and published in CP, presenting in details each step of the model, without publishing data related paleoclimate reconstruction alongside. A very well-known example is the recently published automatization method presented by Winstrup et al. (2012) in order to run automated annual layer counting in ice cores using multiple annually resolved records. This paper was very welcomed by the reviewers in CP, and the method has been successfully applied since then to reconstruct chronologies for many ice core records. We believe the focus of our submitted manuscript is very similar to the one from Winstrup et al., applied to a different problem, but always linked to paleoclimate reconstruction.

It would improve the paper if Kobashi's work could be compared to the results found here, and placed in a larger context. Additionally, it would be helpful if the present work were actually used to reconstruct Greenland temperature over the Holocene, much as Kobashi et al. did. I am somewhat surprised that Kobashi is not a co-author, considering how heavily this work relies on Kobashi et al.'s prior work. The synthetic data looks a lot like Kobashi et al.'s actual data. Why not show the actual data?

As explained in detail in the answer on point (4) for reviewer 2, due to the aim of the paper to describe the algorithm in every detail and in a well-known environment (i.e., using a synthetic dataset as target), we decided not to show the results of the inversion of the GISP2 measurement data within this publication. Furthermore, the paper was criticized because of its length and the amount of figures which makes it impossible to show the description of the fitting algorithm together with the inversion of measurement data in a single publication without the danger of losing the scope on the major issues.

As explained above, our inversion method is entirely new and therefore cannot be considered to rely at all on Kobashi's work, which by the way we very much appreciate. However we fully agree that our method (as Kobashi's method) works only when coupled to a firn densification model which is itself coupled to an ice sheet flow model equipped with heat transfer, such as the Schwander or the Goujon model.

Minor comments:

page 1 line 11 "The presented approach is completely automated..."

We correct for that. The new sentence reads:

"The presented approach is completely automated and leads to a match of the $\delta^{15}\text{N}$ target data in the low permeg level and to related temperature deviations of a few tenths of Kelvin for different data scenarios, showing the robustness of the reconstruction method."

page 1 line 23 "since it represents a time of moderate natural variations prior to anthropogenic disturbance, often referred to as a baseline...."

We correct for that. The new sentence reads:

"Holocene climate variability is of key interest to our society, since it represents a time of moderate natural variations prior to anthropogenic disturbance, often referred to as a baseline for today's increasing greenhouse effect driven by mankind."

page 2 line 6 "The studies of Dahl-Jensen et al. (1998) and Cuffey et al. (1995; 1997) demonstrate the usefulness of inverting the measured borehole temperature profile for surface temperature history...."

We correct for that and added the references. The new sentence reads:

"The studies of Dahl-Jensen et al. (1998) and Cuffey et al. (1995; 1997) demonstrate the usefulness of inverting the measured borehole temperature profile for surface temperature history estimates for the investigated drilling site using a coupled heat- and ice-flow model. "

page 2 line 9 "unable to resolve..."

We correct for that. The new sentence reads:

"Because of smoothing effects due to the nature of heat diffusion within an ice sheet, this method is unable to resolve fast temperature oscillations and leads to a rapid reduction of the time resolution towards the past."

page 3 line 24. It is not clear from the wording here which thermal diffusion sensitivity value was used here. Is it the Grachev and Severinghaus (2003), or the Leuenberge et al. (1999)? This must be clarified. A separate issue is that the Leuenberger et al. value is based on measurements that were made in pure nitrogen, not in air. It is well known, and indeed predicted from theory, that the thermal diffusion sensitivity (and thermal diffusion factor) is larger in pure gases than in air. For example, Grachev and Severinghaus measured these parameters in both pure N₂ and in air, and found a substantial difference between the two (Figure 1). As can be seen in Figure 1, the thermal diffusion factor in pure N₂ is 0.0037 whereas in air it is less than 0.0036. Even more troubling is the fact that the 1960s-era measurements made in pure N₂ by the sources that Leuenberger et al. use disagree well outside the analytical error (0.0035) with the pure-N₂ value of Grachev and Severinghaus, which was made with a modern mass spectrometer. This suggests that the 1960s era measurements by Boersma-Klein and De Vries (1966) were badly in error. Given the primitive technology of that time, this is not a criticism of these workers, but it is clear that their values should not be used for the present study.

We thank the reviewer mentioning that point. Indeed we used a wrong equation here, which was a relic from an older version of the paper. However, all calculations have been performed using the thermal diffusion sensitivity from Grachev and Severinghaus (2003). We changed Eq. (4) to:

$$\alpha_T = \left(8.656 - \frac{1323 \text{ K}}{\bar{T}} \right) \cdot 10^{-3}$$

page 3 line 26 "The firn model used here behaves purely as a forward model,...."

We correct for that. The new sentence reads:

"The firn model used here behaves purely as a forward model, which means that for the given input time series the output parameters (here finally $\delta^{15}\text{N}_{\text{mod}}(t)$) can be calculated, but it is not easily possible to reconstruct from measured isotope data the related surface temperature or accumulation rate histories."

page 4 line 3 You must say which ice core was used here. Is it GISP2?

We correct for that. The new sentence reads:

“In this study, accumulation rate data from Cuffey and Clow (1997) for the GISP2 ice core, adapted to the GICC05 chronology, is used (Rasmussen et al., 2008; Seierstad et al., 2014).”

References:

- Andersen, K. K., Azuma, N., Barnola, J.-M., Bigler, M., Biscaye, P., Caillon, N., Chappellaz, J., Clausen, H. B., Dahl-Jensen, D., Fischer, H., Flückiger, J., Fritzsche, D., Fujii, Y., Goto-Azuma, K., Grønbold, K., Gundestrup, N. S., Hansson, M., Huber, C., Hvidberg, C. S., Johnsen, S. J., Jonsell, U., Jouzel, J., Kipfstuhl, S., Landais, A., Leuenberger, M., Lorrain, R., Masson-Delmotte, V., Miller, H., Motoyama, H., Narita, H., Popp, T., Rasmussen, S. O., Raynaud, D., Rothlisberger, R., Ruth, U., Samyn, D., Schwander, J., Shoji, H., Siggard-Andersen, M.-L., Steffensen, J. P., Stocker, T., Sveinbjörnsdóttir, A. E., Svensson, A., Takata, M., Tison, J.-L., Thorsteinsson, T., Watanabe, O., Wilhelms, F. and White, J. W. C.: High-resolution record of Northern Hemisphere climate extending into the last interglacial period, *Nature*, 431(7005), 147–151, doi:10.1038/nature02805, 2004.
- Buizert, C., Martinerie, P., Petrenko, V. V., Severinghaus, J. P., Trudinger, C. M., Witrant, E., Rosen, J. L., Orsi, A. J., Rubino, M., Etheridge, D. M., Steele, L. P., Hogan, C., Laube, J. C., Sturges, W. T., Levchenko, V. A., Smith, A. M., Levin, I., Conway, T. J., Dlugokencky, E. J., Lang, P. M., Kawamura, K., Jenk, T. M., White, J. W. C., Sowers, T., Schwander, J. and Blunier, T.: Gas transport in firn: Multiple-tracer characterisation and model intercomparison for NEEM, Northern Greenland, *Atmos. Chem. Phys.*, 12(9), 4259–4277, doi:10.5194/acp-12-4259-2012, 2012.
- Buizert, C., Sowers, T. and Blunier, T.: Assessment of diffusive isotopic fractionation in polar firn, and application to ice core trace gas records, *Earth Planet. Sci. Lett.*, 361, 110–119, doi:10.1016/j.epsl.2012.11.039, 2013.
- Cuffey, K. M. and Clow, G. D.: Temperature, accumulation, and ice sheet elevation in central Greenland through the last deglacial transition, *J. Geophys. Res. Ocean.*, 102(C12), 26383–26396, doi:10.1029/96JC03981, 1997.
- Goujon, C., Barnola, J.-M. and Ritz, C.: Modeling the densification of polar firn including heat diffusion: Application to close-off characteristics and gas isotopic fractionation for Antarctica and Greenland sites, *J. Geophys. Res. Atmos.*, 108(D24), n/a-n/a, doi:10.1029/2002JD003319, 2003.
- Guillevic, M.: PhD thesis., 2013.
- Guillevic, M., Bazin, L., Landais, A., Kindler, P., Orsi, A., Masson-Delmotte, V., Blunier, T., Buchardt, S. L., Capron, E., Leuenberger, M., Martinerie, P., Prié, F. and Vinther, B. M.: Spatial gradients of temperature, accumulation and $\delta^{18}\text{O}$ - ice in Greenland over a series of Dansgaard-Oeschger events, *Clim. Past*, 9(3), 1029–1051, doi:10.5194/cp-9-1029-2013, 2013.
- Hedges L. V., O. I.: *Statistical methods for meta-analysis*, Academic Press, San Diego., 1985.
- Johnsen, S. J., Dahl-Jensen, D., Gundestrup, N., Steffensen, J. P., Clausen, H. B., Miller, H., Masson-Delmotte, V., Sveinbjörnsdóttir, A. E. and White, J.: Oxygen isotope and palaeotemperature records from six Greenland ice-core stations: Camp Century, Dye-3, GRIP, GISP2, Renland and NorthGRIP, *J. Quat. Sci.*, 16(4), 299–307, doi:10.1002/jqs.622, 2001.
- Kindler, P., Guillevic, M., Baumgartner, M., Schwander, J., Landais, A. and Leuenberger, M.: Temperature reconstruction from 10 to 120 kyr b2k from the NGRIP ice core, *Clim. Past*, 10(2), 887–902, doi:10.5194/cp-10-887-2014, 2014.
- Kobashi, T., Severinghaus, J. P. and Kawamura, K.: Argon and nitrogen isotopes of trapped air in the GISP2 ice core during the Holocene epoch (0-11,500 B.P.): Methodology and implications for gas loss processes, *Geochim. Cosmochim. Acta*, 72(19), 4675–4686, doi:10.1016/j.gca.2008.07.006, 2008.
- Martinerie, P., Lipenkov, V. Y., Raynaud, D., Chappellaz, J., Barkov, N. I. and Lorius, C.: Air content paleo record in the Vostok ice core (Antarctica): A mixed record of climatic and glaciological parameters, *J. Geophys. Res.*, 99(D5), 10565, doi:10.1029/93JD03223, 1994.
- Meese, D. A., Alley, R. B., Flacco, R. J., Germani, M. S., Gow, A. J., Grootes, P. M., Illing, M., Mayewski, P. A., Morrison, M. C., Ram, M., Taylor, K., Yang, Q. and Zielinski, G. A.: Preliminary depth-age scale of the GISP2 ice core. [online] Available from: <https://scholar.google.ch/scholar?q=Meese%2C+D.A.%2C+R.B.+Alley%2C+R.J.+Fiacco%2C+M.S.+Germani%2C+A.J.+Gow%2C+P.M.+Grootes%2C+M.+Illing%2C+P.A.+Mayewski%2C+M.C.+Morrison%2C+M.+Ram%2C+K.C.+Taylor%2C+Q.+Yang%2C+and+G.A.+Zielinski.+1994.+Preliminary+depth-ag> (Accessed 21 March 2017), 1994.
- Rasmussen, S. O., Bigler, M., Blockley, S. P., Blunier, T., Buchardt, S. L., Clausen, H. B., Cvijanovic, I., Dahl-Jensen, D., Johnsen, S. J., Fischer, H., Gkinis, V., Guillevic, M., Hoek, W. Z., Lowe, J. J., Pedro, J. B., Popp, T., Seierstad, I. K., Steffensen, J. P., Svensson, A. M., Vallenga, P., Vinther, B. M., Walker, M. J. C., Wheatley, J. J. and Winstrup, M.: A stratigraphic framework for abrupt climatic changes during the Last Glacial period based on three synchronized Greenland ice-core records: Refining and extending the INTIMATE event stratigraphy, *Quat. Sci. Rev.*, 106, 14–28, doi:10.1016/j.quascirev.2014.09.007, 2014.
- Rosen, J. L., Brook, E. J., Severinghaus, J. P., Blunier, T., Mitchell, L. E., Lee, J. E., Edwards, J. S. and Gkinis, V.: An ice core record of near-synchronous global climate changes at the Bølling transition, *Nat.*

- Geosci., 7(6), 459–463, doi:10.1038/ngeo2147, 2014.
- Schwander, J., Sowers, T., Barnola, J. M., Blunier, T., Fuchs, A. and Malaizé, B.: Age scale of the air in the summit ice: Implication for glacial-interglacial temperature change, *J. Geophys. Res.*, 102(D16), 19483–19493, doi:10.1029/97JD01309, 1997.
- Seierstad, I. K., Abbott, P. M., Bigler, M., Blunier, T., Bourne, A. J., Brook, E., Buchardt, S. L., Buizert, C., Clausen, H. B., Cook, E., Dahl-Jensen, D., Davies, S. M., Guillevic, M., Johnsen, S. J., Pedersen, D. S., Popp, T. J., Rasmussen, S. O., Severinghaus, J. P., Svensson, A. and Vinther, B. M.: Consistently dated records from the Greenland GRIP, GISP2 and NGRIP ice cores for the past 104ka reveal regional millennial-scale $\delta^{18}\text{O}$ gradients with possible Heinrich event imprint, *Quat. Sci. Rev.*, 106, 29–46, doi:10.1016/j.quascirev.2014.10.032, 2014.
- Severinghaus, J. P.: Winter Sampling of Shallow Firn Air at the South Pole to Understand Processes Affecting Firn Atmospheric Histories and Ice Core Gas Records, icebubbles.ucsd.edu [online] Available from: https://www.researchgate.net/profile/Jeff_Severinghaus/publication/253977940_Winter_Sampling_of_Shallow_Firn_Air_at_the_South_Pole_to_Understand_Processes_Affecting_Firn_Atmospheric_Histories_and_Ice_Core_Gas_Records/links/543bfd600cf24a6ddb97d32a.pdf (Accessed 5 September 2017), 1998.
- Severinghaus, J. P., Albert, M. R., Courville, Z. R., Fahnestock, M. A., Kawamura, K., Montzka, S. A., Mühle, J., Scambos, T. A., Shields, E., Shuman, C. A., Suwa, M., Tans, P. and Weiss, R. F.: Deep air convection in the firn at a zero-accumulation site, central Antarctica, *Earth Planet. Sci. Lett.*, 293(3–4), 359–367, doi:10.1016/j.epsl.2010.03.003, 2010.
- Winstrup, M., Svensson, A. M., Rasmussen, S. O., Winther, O., Steig, E. J. and Axelrod, A. E.: An automated approach for annual layer counting in ice cores, *Clim. Past*, 8(6), 1881–1895, doi:10.5194/cp-8-1881-2012, 2012.

Novel automated inversion algorithm for ice core based temperature reconstructions – a synthetic data study for Holocene $\delta^{15}\text{N}$ data reconstruction using gas isotopes from ice cores

Michael Döring^{1,2*} and Markus Leuenberger^{1,2}

¹Climate and Environmental Physics, University of Bern, Switzerland

²Oeschger Centre for Climate Change Research (OCCR), Bern, Switzerland

*Correspondence to: Michael Döring (doering@climate.unibe.ch)

Formatiert: Englisch (Großbritannien)

Keywords: temperature reconstruction, ice core, nitrogen isotope, argon isotope, inverse model, firm model

Abstract. ~~We present a novel approach for reconstructing the Holocene surface Greenland past~~ temperature ~~histories~~ history can be reconstructed by forcing the output of a firm densification and heat diffusion model to fit ~~nitrogen~~ multiple gas isotope data ($\delta^{15}\text{N}$ or $\delta^{40}\text{Ar}$ or $\delta^{15}\text{N}_{\text{excess}}$) extracted from ancient air in Greenland ice cores. ~~The~~ We present here a novel methodology to solve this inverse problem, by designing a fully automated algorithm. To demonstrate the performance of this novel approach ~~is demonstrated using, we begin by intentionally constructing synthetic data~~ temperature histories and associated $\delta^{15}\text{N}$ datasets, mimicking real Holocene data that we use as “true values” (targets) to be compared to the output of the algorithm. This allows us to quantify uncertainties originating from the algorithm itself. The presented approach works completely automated and leads to a match of the $\delta^{15}\text{N}$ target data in the low permeg level and to related temperature deviations ~~therefore minimizes the “subjective” impact of a few tenths of Kelvin for different data scenarios, showing the robustness of the manual parameter tuning leading to reproducible temperature estimates. In contrast to many other ice core based temperature reconstruction method. The obtained, final mismatches follow a symmetric, standard distribution function. 95% of the mismatches compared to the synthetic target data are in an envelope in between 3.0–6.3 permeg for $\delta^{15}\text{N}$ and 0.23–0.51 K for temperature (2σ , respectively).~~ methods, the presented approach is completely independent from ice core stable water isotopes, providing the opportunity to validate water isotope based reconstructions or reconstructions where water isotopes are used together with $\delta^{15}\text{N}$ or $\delta^{40}\text{Ar}$. We solve the inverse problem $T(\delta^{15}\text{N})$ by using a combination of a Monte Carlo ~~sampling~~ based iterative approach and ~~quantitative data~~ the analysis of remaining mismatches between modelled and target data, based on cubic spline filtering of random numbers ~~and as well as the measured~~ laboratory determined temperature sensitivity for nitrogen isotopes. Additionally, the presented reconstruction approach was tested by fitting measured $\delta^{40}\text{Ar}$ and $\delta^{15}\text{N}_{\text{excess}}$ data ~~(Döring et al., in prep.),~~ which leads as well to same ~~a~~ robust agreement between modelled and measurement data. ~~measured data. The obtained final mismatches follow a symmetric standard distribution function. For the synthetic data study, 95 % of the mismatches compared to the synthetic target data are in an envelope between 3.0 permeg to 6.3 permeg for $\delta^{15}\text{N}$ and 0.23 K to 0.51 K for temperature (2σ , respectively).~~ In addition to Holocene

temperature reconstructions, the fitting approach can also be used for glacial temperature reconstructions (~~Döring et al., in prep.~~) and it is reasonable to adapt the approach for model inversions of other non-linear physical processes. This is shown by high quality fitting of NGRIP $\delta^{15}\text{N}$ data for two Dansgaard-Oeschger events using the presented approach, leading to results comparable to other studies.

5 1 Introduction

Holocene climate variability is of key interest to our society, since it represents ~~the rather constant~~ a time ~~window with~~of moderate natural variations: prior to anthropogenic disturbance, often referred to as a baseline for today's increasing greenhouse effect driven by mankind. Yet, high resolution studies are still very sparse and therefore limit the investigation of decadal and partly even centennial climate variations over the course of the Holocene. One of the first studies about changes in the Holocene climate was conducted in the early 1970s by Denton and Karle'n (1973). The authors investigated rapid changes in glacier extents around the globe potentially resulting from variations of Holocene climatic conditions. Mayewski et al. (2004) ~~used this data as the base of a multiproxy study identifying rapid climate changes (so-called RCCs) globally distributed over the whole Holocene time period. Although not all proxy data are showing an equal behaviour in timing and extent during the quasi-periodic RCC patterns, the authors found evidence for a highly variable Holocene climate controlled by multiple mechanisms, which significantly affects ecosystems (Beaulieu et al., 2017; Crausbay et al., 2017; Pál et al., 2016) and human societies~~ used this data as the base of a multiproxy study identifying rapid climate changes (so called RCCs) globally distributed over the whole Holocene time period. Although not all proxy data are showing an equal behaviour in timing and extent during the quasi-periodic RCC patterns, the authors found evidence for a highly variable Holocene climate controlled by multiple mechanisms, which significantly affects ecosystems (Pál et al., 2016; Beaulieu et al., 2017; Crausbay et al., 2017) and human societies (Holmgren et al., 2016 ; Lespez, L. et al., 2016). ~~Precise high resolution temperature estimates can contribute significantly to the understanding of these mechanisms. Ice core proxy data offer multiple paths for reconstructing past climate and temperature variability. The study of Dahl Jensen et al. (1998) exemplarily demonstrates the usefulness of inverting the measured borehole temperature profile to surface temperature estimates for the investigated drilling site using a coupled heat and ice flow model. Because of smoothing effects due to the nature of heat diffusion within an ice sheet, this method is unable to dissolve fast temperature oscillations and leads to a rapid reduction of the time resolution towards the past. Another approach for reconstructing past temperature is based on the calibration of stable water isotopes of oxygen and hydrogen ($\delta^{18}\text{O}_{\text{H}_2\text{O}}$, $\delta\text{D}_{\text{H}_2\text{O}}$) from ice core water samples assuming a constant (and mostly linear) relationship between temperature and isotope values due to fractionation of evaporation and rainout processes for a certain time period (Stuiver et al., 1995 ; Johnsen et al., 2001). This method provides a rather robust tool for reconstructing past temperature for times where large temperature excursions occur (Dansgaard-Oeschger events, Glacial-Interglacial transitions (Johnsen et al., 1992; Dansgaard et al., 1982)). However, in the Holocene where Greenland temperature variations are comparatively small, seasonal changes of precipitation as well as of evaporation conditions at the source region~~

contribute possibly more to water isotope data variations (Kindler et al., 2014; Huber et al., 2006; Werner et al., 2001). A relatively new method for ice core based temperature reconstructions uses the thermal fractionation of stable isotopes of air compounds (nitrogen and argon) within a firn layer of an ice sheet (Severinghaus et al., 2001; Severinghaus et al., 1998; Kobashi et al., 2011; Kindler et al., 2014; Huber et al., 2006). The measured nitrogen and argon isotope records of air enclosed in bubbles in an ice core can be used as a paleothermometer due to (i) the stability of isotopic compositions of nitrogen and argon in the atmosphere at orbital timescales and (ii) the fact that changes are only driven by firn processes (Severinghaus et al., 1998; Mariotti, 1983; Leuenberger et al., 1999). To robustly reconstruct the surface temperature for a given drilling site, the use of firn models describing gas and heat diffusion throughout the ice sheet is necessary for decomposing the gravitational from the thermal diffusion influence on the isotope signals. This work addresses two issues relevant for nitrogen and argon isotope based temperature reconstructions. First, we introduce a novel, entirely automated approach for inverting nitrogen isotope data to surface temperature estimates forcing the output of a firn densification and heat diffusion model to fit the nitrogen isotope data. And second, we investigate, how accurate can this be done in the framework of the used model, by examining the approach on different synthetic nitrogen isotope and temperature scenarios.

. Precise high resolution temperature estimates can contribute significantly to the understanding of these mechanisms. Ice core proxy data offer multiple paths for reconstructing past climate and temperature variability. The studies of Cuffey et al. (1995; 1997) and Dahl-Jensen et al. (1998) demonstrate the usefulness of inverting the measured borehole temperature profile for surface temperature history estimates for the investigated drilling site using a coupled heat- and ice-flow model. Because of smoothing effects due to heat diffusion within an ice sheet, this method is unable to resolve fast temperature oscillations and leads to a rapid reduction of the time resolution towards the past. Another approach to reconstruct past temperature is based on the calibration of stable water isotopes of oxygen and hydrogen ($\delta^{18}\text{O}_{\text{ice}}$, $\delta\text{D}_{\text{ice}}$) from ice core water samples assuming a constant (and mostly linear) relationship between temperature and water isotopic composition due to fractionation effects during ocean evaporation, cloud formation and snow and ice precipitation (Stuiver et al., 1995; Johnsen et al., 2001). This method provides a rather robust tool for reconstructing past temperature for times where large temperature excursions occur (Dansgaard-Oeschger events, Glacial-Interglacial transitions (Dansgaard et al., 1982; Johnsen et al., 1992)). However, in the Holocene where Greenland temperature variations are comparatively small, seasonal changes of precipitation as well as of evaporation conditions at the source region contribute possibly more to water isotope data variations (Werner et al., 2001; Huber et al., 2006; Kindler et al., 2014;). A relatively new method for ice core based temperature reconstructions uses the thermal fractionation of stable isotopes of air compounds (nitrogen and argon) within a firn layer of an ice sheet (Severinghaus et al., 1998; Severinghaus et al., 2001; Huber et al., 2006; Kobashi et al., 2011; Kindler et al., 2014). The measured nitrogen and argon isotope records of air enclosed in bubbles in an ice core can be used as a paleothermometer due to (i) the stability of isotopic compositions of nitrogen and argon in the atmosphere at orbital timescales and (ii) the fact that changes are only driven by firn processes (Mariotti, 1983; Severinghaus et al., 1998; Leuenberger et al., 1999). To robustly reconstruct the surface temperature for a given drilling site, the use of firn models

describing gas and heat diffusion throughout the ice sheet is necessary for decomposing the gravitational from the thermal diffusion influence on the isotope signals.

This work addresses two issues relevant for nitrogen and argon isotope based temperature reconstructions. First, we introduce a novel, entirely automated approach for inverting gas isotope data to surface temperature estimates. For that, we force the output of a firm densification and heat diffusion model to fit gas isotope data. This methodology can be used for many different optimization tasks not restricted to ice core data. As we will show, the approach works besides $\delta^{15}\text{N}$ for all relevant gas isotope quantities ($\delta^{15}\text{N}$, $\delta^{40}\text{Ar}$, $\delta^{15}\text{N}_{\text{excess}}$) and for Holocene and glacial data as well. Furthermore, the possibility of fitting all relevant gas isotope quantities, individually or combined, makes it possible for the first time to validate the temperature solution gained from one single isotope species by comparison to the solution calculated from other isotope quantities. This approach is a completely new method which enables the automated fitting of gas isotope data without any manual tuning of parameters, minimizing any potential “subjective” impacts on temperature estimates as well as working hours. Also, except for the model spin-up, the presented temperature reconstruction approach is completely independent from stable water isotopes ($\delta^{18}\text{O}_{\text{ice}}$, $\delta\text{D}_{\text{ice}}$), which provides the opportunity to validate water isotope based reconstructions (e.g. Masson-Delmotte, 2005) or reconstructions where water isotopes are used together with $\delta^{15}\text{N}$ or $\delta^{40}\text{Ar}$ (e.g. Landais et al., 2004; Huber et al., 2006; Capron et al., 2010). To our knowledge, there are only two other reconstruction methods independent from stable water isotopes that have been applied to Holocene gas isotope data, without a priori assumption on the shape of a temperature change. The studies from Kobashi et al. (2008a, 2017) use the second order parameter $\delta^{15}\text{N}_{\text{excess}}$ to calculate firm temperature gradients, which are later temporally integrated from past to future over the time series of interest using the firm densification and heat diffusion model from Goujon et al. (2003). Additionally Orsi et al. (2014) use a linearized firm model approach together with $\delta^{15}\text{N}$ and $\delta^{40}\text{Ar}$ data to extract surface temperature histories. As both methods rely on $\delta^{15}\text{N}$ together with $\delta^{40}\text{Ar}$, they do not offer the possibility to validate one isotope based solution against the other. Also these two approaches can only be applied to ice cores where both isotope quantities are measured together with a sufficient precision.

Second, we investigate the accuracy of our novel fitting approach by examining the method on different synthetic nitrogen isotope and temperature scenarios. The aim of this work is to study the uncertainties emerging from the algorithm itself. Furthermore the focal question in this study is: what is the minimal mismatch in $\delta^{15}\text{N}$ for Holocene like data we can reach and what is the implication for the final temperature mismatches. Studying and moreover answering these questions makes it mandatory to create well defined $\delta^{15}\text{N}$ targets and related temperature histories. It is impossible to answer these questions without using synthetic data in a methodology study. The aim is to evaluate the accuracy and associated uncertainty of the inverse method itself to then later apply this method to real $\delta^{15}\text{N}$, $\delta^{40}\text{Ar}$ or $\delta^{15}\text{N}_{\text{excess}}$ datasets, for which of course the original driving temperature histories are unknown.

2. Methods and data

2.1 Firn densification and heat diffusion model

The surface temperature reconstruction relies on firn densification combined with gas and heat diffusion (Severinghaus et al., 1998). In this study, the firn densification and heat diffusion model, from now on referred to as firn model, developed by Schwander et al. (1997) is used to reconstruct firn parameters for calculating synthetic $\delta^{15}\text{N}$ values depending on the input time series. It is a semi-empirical model based on the work of Herron and Langway (1980), Barnola et al. (1991) Barnola et al. (1991), and implemented using the Crank and Nicholson algorithm (Crank, 1975) and was also used for the temperature reconstructions by Huber et al. (2006) and Kindler et al. (2014). Besides surface temperature time series, accurate accumulation rate data is needed to run the model (Fig. 01). The model then calculates the densification and heat diffusion history of the firn layer and provides parameters for calculating the fractionation of the nitrogen isotopes for each time step, according to the following equations:

$$\delta^{15}N_{\text{grav}}(z_{\text{LID}}, t) = \left(e^{\frac{\Delta m \cdot g \cdot z_{\text{LID}}(t)}{R \cdot T(t)}} - 1 \right) \delta^{15}N_{\text{grav}}(z_{\text{LID}}, t) = \left(e^{\frac{\Delta m \cdot g \cdot z_{\text{LID}}(t)}{R \cdot T(t)}} - 1 \right) \cdot 1000 \quad (1)$$

$$\delta^{15}N_{\text{therm}}(t) = \left[\left(\frac{T_{\text{surf}}(t)}{T_{\text{bottom}}(t)} \right)^{\alpha_T} - 1 \right] \delta^{15}N_{\text{therm}}(t) = \left[\left(\frac{T_{\text{surf}}(t)}{T_{\text{bottom}}(t)} \right)^{\alpha_T} - 1 \right] \cdot 1000 \quad (2)$$

$$\delta^{15}N_{\text{mod}}(t) = \delta^{15}N_{\text{grav}}(t) + \delta^{15}N_{\text{therm}}(t) \delta^{15}N_{\text{mod}}(t) = \delta^{15}N_{\text{grav}}(t) + \delta^{15}N_{\text{therm}}(t) \quad (3)$$

$\delta^{15}N_{\text{grav}}(t)$ is the component of the isotopic fractionation due to the gravitational settling (Craig et al., 1988; Schwander, 1989) and depends on the lock-in-depth $z_{\text{LID}}(t)$ (depth where the density of the firn reaches a certain value, based on the empirical formula from Martinerie et al. (1994), which is the density where the porosity of the firn column is low enough, so the gas diffusion is negligible) and the mean firn temperature $\bar{T}(z_{\text{LID}})$ $z_{\text{LID}}(t)$ and the mean firn temperature $\bar{T}(t)$ (Leuenberger et al., 1999). g is the acceleration constant, Δm the molar mass difference between the heavy and light isotopes (equals one gram for nitrogen) and R the ideal gas constant, 10^{-3} kg for nitrogen) and R the ideal gas constant. z_{LID} is defined as a density threshold ρ_{LID} , which is slightly sensitive to surface temperature, following the formula from Martinerie et al. (1994), with a small offset correction of 14 kg m^{-3} to account for the presence of a non-diffusive zone (Schwander et al., 1997):

$$\rho_{\text{LID}}(\text{kg} \cdot \text{m}^{-3}) = \frac{1}{\frac{1}{\rho_{\text{ice}}} - 6.95 \cdot 10^{-7} \cdot \bar{T} - 4.3 \cdot 10^{-5}} - 14 \quad (4)$$

where

$$\rho_{\text{ice}}(\text{kg} \cdot \text{m}^{-3}) = 916.5 - 0.14438 \cdot \bar{T} - 1.5175 \cdot 10^{-4} \cdot \bar{T}^2 \quad (5)$$

The thermal fractionation component of the $\delta^{15}\text{N}$ signal (Severinghaus et al., 1998) is calculated using Eq. (2), where $T_{\text{surf}}(t)$ and $T_{\text{bottom}}(t)$ stand for the temperatures at the top and the bottom of the diffusive firn layer. In contrast to $T_{\text{surf}}(t)$ which is an

input parameter for the model, $T_{\text{bottom}}(t)$ is calculated by the model for each time step. The thermal diffusion constant α_T was measured by Grachev and Severinghaus (2003) for nitrogen, ~~expressed there as Ω , (see Eq. (6))~~, and closely matches the value used by Leuenberger et al. (1999) based on measurements of Boersma-Klein and De Vries (1966):

$$\alpha_T = 4.61198 \cdot 10^{-3} \cdot \ln(\bar{T}/113.65K) \quad (4)$$

$$\alpha_T = \left(8.656 - \frac{1323 K}{\bar{T}} \right) \cdot 10^{-3} \quad (6)$$

The ~~used~~ firm model used here behaves purely as a ~~sheer~~ forward model, which means that for the given input time series the output parameters (here finally $\delta^{15}N_{\text{mod}}(t)$) can be calculated, but it is not easily possible to construct from measured isotope data the related surface temperature or accumulation rate histories ~~(Fig. 01)~~. The goal of the presented study is an automatization of this inverse modelling procedure for the reconstruction of the rather small Holocene temperature variations.

2.2 Measurement, input data and time scale

Accumulation rate data: Besides surface temperatures, accumulation rate data is needed to drive the firm model. ~~In this study, accumulation rate data from Cuffey and Clow (1997), adapted to the GICC05 chronology, is used~~ In this study we use the original accumulation rate, reconstructed in Cuffey and Clow (1997) produced using an ice flow model adapted to the GISP2 location, but adapted to the GICC05 chronology (Rasmussen et al., 2008; Seierstad et al., 2014). From three accumulation rate scenarios Originally, the accumulation rate used to feed the ice flow model was optimised in order to match the time scale from Meese et al. (1994) for the Holocene, based on annual layer counting. Seierstad et al. (2014) transferred the GISP2 chronology to the GICC05 reference timeframe using multiple match points to the NGRIP and GRIP ice cores, both already on GICC05. We used these match points and modified the GISP2 ages in between match points linearly in order to match exactly the GICC05 duration for the considered interval duration. This way, the detailed GISP2 annual layer counting information is kept, but is only stretched/compressed in time. This was done for all intervals in between two match points. The accumulation data were then re-calculated accordingly as obviously this is needed in order to keep the same total amount of ice accumulated at the GISP2 site. From the three accumulation rate scenarios reconstructed in Cuffey and Clow (1997) and adapted here to the GICC05 chronology, the intermediate one is chosen (red curves in Fig. S01). Since the differences between the scenarios (Fig. S01) are not important for the evaluation of the reconstruction approach, they are not taken into account for this study.

$\delta^{18}O_{\text{ice}}$ data: Oxygen isotope data from the GISP2 ice core water samples measured at the University of Washington's Quaternary Isotope Laboratory is used to construct the surface temperature input of the model spin-up (12-35 kyr b2k, see Sect. 2.4) (Grootes and Stuiver, 1997; Stuiver et al., 1995; Meese et al., 1994; Steig et al., 1994; Grootes et al., 1993), yr to 35 kyr b2k, see Sect. 2.3.1) (Grootes et al., 1993; Meese et al., 1994; Steig et al., 1994; Stuiver et al., 1995; Grootes and Stuiver, 1997).

Formatiert: Englisch (Großbritannien)

Formatiert: Englisch (Großbritannien)

Formatiert: Englisch (Großbritannien)

Feldfunktion geändert

Feldfunktion geändert

Formatiert: Englisch (Großbritannien)

Time scale: For the entire study the GICC05 chronology is used (Rasmussen et al., 2014; Seierstad et al., 2014). During the whole reconstruction procedure the two input time series (surface temperature and accumulation rate) are split into two parts. The first part ranges from 20 yr to 10520 yr b2k (called “Holocene section”) and the second one from 10520 yr to 35000 yr b2k (“spin-up section”). The ~~whole~~entire accumulation rate input (see Sect. 2.4.1), as well as the spin-up section of the surface temperature input, remain unchanged during the reconstruction procedure.

2.3 Pre study and Sensitivity tests – Search for a transfer function

2.3.1 Static case

To investigate the model behaviour in its static condition (constant temperature and accumulation rate) a set of 408 input scenarios was run by the firm model calculating the $\delta^{15}\text{N}$ outputs for each permutation. The surface temperature inputs were varied in the range of $-60\text{ }^{\circ}\text{C}$ to $-10\text{ }^{\circ}\text{C}$ with 1 K step width and the accumulation rates were changed between 0.10 and 0.45 m/yr in 0.05 m/yr steps leading to 51 times 8 scenarios (Fig. 02a,b). Each input scenario was calculated in a 30 kyr time window to make sure that no spin up effects influence the output $\delta^{15}\text{N}$ data. With the obtained temperature, accumulation and $\delta^{15}\text{N}$ combinations different polynomial surface fits were conducted in order to find a transfer function (Table S01 and Fig. S02) which approximates the static model behaviour in the best possible manner. Figure 02c shows the comparison between the model $\delta^{15}\text{N}$ and the surface polynomial fit using degree 3 in temperature (T in Kelvin) and degree 2 in accumulation rate (Acc) leading to a robust model approximation with a correlation coefficient $r^2 = 0.9997$ and root mean square error (RMSE) of about 4.5 permeg over the investigated model space and shows a non-linear behaviour in $\delta^{15}\text{N}(T)$ and $\delta^{15}\text{N}(Acc)$.

$$\delta^{15}\text{N}(T, Acc) = p_{00} + p_{10} \cdot T + p_{01} \cdot Acc + p_{20} \cdot T^2 + p_{02} \cdot Acc^2 + p_{20} \cdot T^2 + p_{11} \cdot T \cdot Acc + p_{21} \cdot T^2 \cdot Acc + p_{12} \cdot T \cdot Acc^2 \quad (5)$$

The coefficients p_{xy} as well as the 95% confidence are listed in Table S01. Figure S02 shows the correlation coefficients r^2 and RMSE for all two dimensional surface fits which were conducted during this analysis as a function of the polynomial degrees in temperature and accumulation rate (T, Acc). It is trivial that a higher polynomial degree leads to a better approximation. More interesting is the fact that an increase of the polynomial degree in temperature seems to be more important than in accumulation rate, e.g. the polynomial of degree 3 in temperature and degree 1 in accumulation rate leads to an about seven-times smaller RMSE compared to a polynomial with reversed degrees.

2.3.2 Dynamic case

A similar study was conducted to investigate the dynamic model behaviour. Here the accumulation rate data (see Sect. 2.2/2.4 and Fig. A01a) together with the reconstructed Holocene temperature for the GISP2 reconstruction (Döring et al., in prep.) were used as input. Figure 03a shows the 2 dimensional dependence of $\delta^{15}\text{N}(T, Acc)$ and (b) the comparison

between modelled and polynomial fitted $\delta^{15}\text{N}$ for which the same surface fit procedure as used for investigating the static model behaviour was applied. It leads to a much poorer approximation with a correlation coefficient (r^2) of about 0.7, and RMSE of about 34.2 permeg. Coefficients are again listed in Table

~~2.3S01. The visible poorer correlation and larger non-linearity of $\delta^{15}\text{N}(T, \text{Acc})$ highlights the problem of system memory effects documented by the firm model output. This is expected, since the model never reaches an equilibrium state for fast temperature and accumulation rate excursions, which complicates the construction of a robust transfer function in the dynamic case. Because our main goal is to fit the $\delta^{15}\text{N}$ data in the low permeg level, i.e. 0.003 permil to 0.005 permil (level of the measurement uncertainty, (Kobashi et al., 2008)), a polynomial transfer function is not suitable for the dynamic case due to its moderate capability to fit the modelled data. Therefore, we use a combination of Monte Carlo sampling and quantitative data analysis for solving the inverse problem $T(\delta^{15}\text{N})$ as sketched in Fig. 01 and explained in detail in the following section.~~

2.4 Reconstruction approach

The Holocene temperature reconstruction is implemented by the following four steps:

- (i) A prior temperature input (first guess) is constructed, which serves as the starting point for the optimization.
- (ii) A smooth solution which passes through the $\delta^{15}\text{N}$ data (here synthetic target data) is generated following a Monte Carlo approach. It is assumed that the smooth solution contains all long term temperature trends (centuries to millennial) as well as firm column height changes (temperature and accumulation rate dependent) that drive the gravitational background signal in $\delta^{15}\text{N}$.
- (iii) The smooth temperature solution is complemented by superimposing high frequency information directly extracted from the $\delta^{15}\text{N}$ data (here synthetic target data). This step adds short term temperature changes (decadal) in the same time resolution as the data.
- (iv) The gained temperature solution is corrected using information extracted from the mismatch between the synthetic target and modelled $\delta^{15}\text{N}$ time series.

Accumulation rate input:

The raw accumulation rate data for the main part of the spin-up section (12000-yr to 35000 yr b2k) is linearly interpolated to a 20 yr grid and low pass filtered with a 200 yr cut off period (cop) using cubic spline filtering (Enting, 1987). For the Holocene section (20-10520 yr b2k) and the transition part between Holocene and spin-up section (10520-yr to 12000 yr b2k) the raw accumulation rate data is linearly interpolated to a 1 yr grid to obtain equidistant integer point-to-point distances which are necessary for the reconstruction, and to preserve as much information as possible for this time period (Fig. ~~A04a~~S02a). Except for these technical adjustments, the accumulation rate input data remains unmodified, assuming high reliability of this data during the Holocene. ~~This is due to the fact that the~~The accumulation data was gained by indeed

Formatiert: Einzug: Links: 1.27 cm

~~reconstructed using~~ annual layer counting, and ~~the use of~~ a thinning model which should ~~be rather robust~~ lead to maximum relative uncertainty of 10 % for the first 1500 m of the 3000 m ice core (Cuffey and Clow, 1997).

In order to investigate the influence of smoothing of the accumulation rate data on the model outputs, the high resolution accumulation rate dataset in the time window of 20-yr to 12000 yr (Fig. A04aS02a) was low pass filtered with cops between 20 yr and 500 yr, and used to drive the firm model. The surface temperature input was set as constant with a value of -31 °C for this time window. Then, the deviations of the filtered from the unfiltered accumulation rates and model outputs were calculated. Figure A02S03 shows the absolute (I) as well as the relative deviations (II) (relative to the unfiltered scenario) as a function of the ~~cut-off periods~~ cops for the accumulation rate input data, $\delta^{15}\text{N}$, and LID model outputs. Regarding the standard deviation (1σ) of the relative ~~errors~~ accumulation deviations as a measure for the mean deviation of the filtered minus the unfiltered values ~~shows show~~ that ~~the filtering of~~ the accumulation rates leads to a mean deviation of about 20 % between the filtered and unfiltered accumulation rate data, depending on the used cop value (see Fig. A02Ha). ~~In Fig. A02HbS03IIa). We use~~ the mean 99-% quantile ~~for of~~ the same analysis ~~is shown which can serve~~ (Fig. S03IIb) as a measure for the maximum deviation between the filtered and unfiltered values. ~~It is clearly visible that the~~ The filtering clearly leads to a maximum accumulation rate deviation of about 50-%. The comparison of the related deviations in ~~the~~ $\delta^{15}\text{N}$ and LID outputs reveals that the changes in the accumulation rates do not lead to a change in the same order for the model outputs. ~~It can be concluded that~~ Indeed, the filtering of the accumulation rate data leads to deviations of less than 0.6 % and less than 1.5 % for the mean and the maximum ~~$\delta^{15}\text{N}$ and LID~~ deviations respectively (Fig. A02HcS03IIc,d). Therefore, it can be argued that a low pass filtering of the accumulation rates for cops between 20-yr and 500 yr does only have a small impact on the model outputs as long as the major trends are being conserved, because the filtering does not modify the mean accumulation. This result ~~was~~ expected due to the fact that the LID and finally $\delta^{15}\text{N}$ changes are the result of the integration of the accumulation over the whole firm column. The integration time corresponds to the age of the ice at the ~~lock-in depth~~ LID, which is the order of 200 yr for the Holocene in Greenland.

~~Figure A03 shows~~ Finally, we test which fraction of the measured $\delta^{15}\text{N}$ variations can be attributed to accumulation changes. For this, we perform a sensitivity experiment (Fig. S04) where the temperature input was set as a constant value of -31 °C, and used together with the high resolution accumulation rate data (Fig. A04aS02a) to model the LID (Fig. A03aS04a) and $\delta^{15}\text{N}$ (Fig. A03bS04b) values. Due to the absence of temperature changes, only the accumulation rate changes drive the ~~time~~ evolution of the diffusive column height (LID) over time, which modulates the $\delta^{15}\text{N}$ values. Next, the modelled $\delta^{15}\text{N}$ variations are compared to the $\delta^{15}\text{N}$ measurement data (Fig. A05HS06III) (Kobashi et al., 2008) (Kobashi et al., 2008b) to examine the influence of the accumulation rate changes on changes in $\delta^{15}\text{N}$ for two cases. First, for the 8.2k event ~~that is clearly visible in the LID and modelled $\delta^{15}\text{N}$ as well as in the $\delta^{15}\text{N}$ measurement data. The, the~~ signal amplitude in $\delta^{15}\text{N}$ is about three times higher for the measured data compared to the modelled ones (~~measurement~~ measured data: $\Delta\delta^{15}\text{N}_{8.2\text{k, meas}} \approx 60$ permeg, ~~(one permeg equals 10^{-6})~~; modelled data: $\Delta\delta^{15}\text{N}_{8.2\text{k, mod}} \approx 20$ permeg). The comparison of the standard deviations of the ~~measurement~~ measured data with the modelled $\delta^{15}\text{N}$ data for the last 10 kyr (both quantities were normalized with their respective means), shows an even higher deviation of the measured versus the modelled variabilities

by a factor of about eight (~~measurement~~measured data: $\text{std}[\delta^{15}\text{N}_{10\text{kyr, meas}} - \text{mean}(\delta^{15}\text{N}_{10\text{kyr, meas}})] \approx 37$ permeg; modelled data: $\text{std}[\delta^{15}\text{N}_{10\text{kyr, mod}} - \text{mean}(\delta^{15}\text{N}_{10\text{kyr, mod}})] \approx 4.5$ permeg). This analysis supports our assumption that the accumulation rate change history alone cannot fully explain the observed variability in $\delta^{15}\text{N}$ during the Holocene, ~~but~~ and gives limits to an upper limit for the contribution of the accumulation rate to the $\delta^{15}\text{N}$ signal. Therefore, the remaining part of the measured $\delta^{15}\text{N}$ variations has to be related to changes in ~~the~~ surface temperature ~~in order to complement the $\delta^{15}\text{N}$ signal.~~

Surface temperature spin-up:

The surface temperature history of the spin-up section (Fig. ~~A01bS02b~~) is obtained by calibrating the filtered and interpolated $\delta^{18}\text{O}_{\text{ice}}$ data (Eq. ~~6~~) (7) using the values for the temperature sensitivity $\alpha_{18\text{O}}$ and offset β found by Kindler et al. (2014) for the NGRIP ice core assuming a linear relationship of $\delta^{18}\text{O}_{\text{ice}}$ with temperature.

$$T_{\text{spin}}(t) = \frac{1}{\alpha_{18\text{O}}(t)} \cdot [\delta^{18}\text{O}_{\text{ice}}(t) + 35.2 \text{‰}] - 31.4^\circ\text{C} + \beta(t) \quad (6)$$

$$T_{\text{spin}}(t) = \frac{1}{\alpha_{18\text{O}}(t)} \cdot [\delta^{18}\text{O}_{\text{ice}}(t) + 35.2 \text{‰}] - 31.4^\circ\text{C} + \beta(t) \quad (7)$$

The values 35.2 ‰ and -31.4°C are modern-time parameters for the GISP2 site (Schwander et al., 1997; Grootes and Stuiver, 1997). The raw $\delta^{18}\text{O}_{\text{ice}}$ data is filtered and interpolated in the same way as the accumulation rate data for the spin-up part.

The spin-up is needed to bring the firm model to a well-defined starting condition that takes possible memory effects (influence of earlier conditions) of firm states into account.

Generating synthetic target data:

In order to develop and evaluate the presented approach algorithm, eight temperature scenarios were constructed and used to model synthetic $\delta^{15}\text{N}$ data, which serve later on as ~~the~~ targets for the reconstruction approach. From these eight synthetic surface temperature and related $\delta^{15}\text{N}$ scenarios (S1-S5 and H1-H3), three data sets (later called Holocene like scenarios H1-H3) were constructed in such a way that the resulting $\delta^{15}\text{N}$ time series are very close to the $\delta^{15}\text{N}$ values measured by Kobashi et al. (2008) (2008) in terms of variability (amplitudes) and frequency (data resolution) of the GISP2 nitrogen isotope data (Fig. ~~A04S05~~, Fig. ~~A05S06~~).

The synthetic surface temperature scenarios S1-S5 are created by generating a smooth temperature time series ($T_{\text{syn, smooth}}$) analogous to the Monte Carlo part of the reconstruction procedure for only one iteration step (see Sect. ~~2.43.2~~). The values for the cut-off period (cop) used for the filtering of the random values, and the s values (standard deviation of the random values, see Sect. 2.3.2) for the first 5 scenarios can be found in ~~Table S02~~ table S01. The smooth temperatures (Fig. ~~A04S05I~~) are calculated on a 20 yr grid, which is nearly similar to the time resolution of the GISP2 $\delta^{15}\text{N}$ measurement values of about 17 yr (Kobashi et al., 2008) (Kobashi et al., 2008b). For the Holocene like scenarios, the smooth temperature time series were generated from the temperature reconstruction for the GISP2 $\delta^{15}\text{N}$ data (~~Döring et al., in prep.~~) not shown here. The final Holocene surface temperature ~~from Döring et al. (in prep.) solution~~ was filtered with a 100 yr cut-off period cop to obtain the smooth temperature scenario.

Following this, high frequency information is added to the smoothed ~~temperatures,~~ temperature histories. A set of normally distributed random numbers with a zero mean and a standard deviation (1σ) of 1 K for ~~the~~ scenarios S1-S5 and 0.3 K for ~~the~~ Holocene like scenarios H1-H3 is generated on the same 20 yr grid and added up to the smooth temperature time series. Finally, the resulting synthetic target temperature scenarios (Fig. ~~A04HS05II~~, Fig. ~~A05HS06I~~) are linearly interpolated to a 1 yr grid.

~~The~~ These synthetic temperatures are combined with the spin-up temperature and are used together with the accumulation rate input to feed the firm model. From the model output the synthetic $\delta^{15}\text{N}$ targets are calculated according to ~~See~~ section 2.1. The firm model output provides ice age as well as gas age information. The final synthetic $\delta^{15}\text{N}$ target time series (Fig. ~~A04HS05III~~, Fig. ~~A05HS06II~~) are set intentionally on the ice age scale to mirror ~~measurement~~ measured data, because no prior information is available for the gas-ice age difference (Δ age) for ice core data.

2.43.1 Prior input (step 1)

The starting point of the optimization procedure is the first guess. To construct the first guess temperature input, a constant temperature of about -29.6°C is used for the complete Holocene section, which corresponds to the last value of the temperature spin-up (Fig. ~~A01b~~). ~~During the next step of the optimization, the prior temperature input is iteratively changed following a Monte Carlo approach.~~ S02b.

2.43.2 Monte Carlo type input generator - Generating smooth solutions (step 2)

During the second step of the optimization, the prior temperature input from step 1 is iteratively changed following a Monte Carlo approach. The basic idea of the Monte Carlo approach is to generate smooth temperature inputs by low-pass filtering uniformly distributed random values, and to superimpose this signal ~~to~~ on the prior input. Then, the new input is fed to the firm model and the mismatch ~~D~~ D_{mc} ~~in~~ between the modelled $\delta^{15}\text{N}$ signal X_{mod} , calculated from the model output, and the synthetic $\delta^{15}\text{N}$ target values X_{syn}, X_{target} is computed. ~~(note that X equals $\delta^{15}\text{N}$ during the Monte Carlo part, whereas for the later analysis of the mismatches of $\delta^{15}\text{N}$ or temperature, X equals $\delta^{15}\text{N}$ or temperature marked by an additional index on “D”)~~

$$D = D_{mc} = \frac{1}{n} \sum_{i=1}^n |D_i| = \frac{1}{n} \sum_{i=1}^n |X_{target,i} - X_{mod,i}| \quad (78)$$

~~D~~ D_{mc} serves as the criterion which is minimised during the optimization in step 2. If the mismatch decreases compared to the prior input, the new input is saved and used as new guess. This procedure is repeated until convergence is achieved.

Table 01 lists the number of improvements and iterations performed for the different synthetic datasets. The perturbation of the current guess ~~$(T_g(t))T_g(t)$~~ is conducted in the following way: Let $\vec{T}_g = T_g(t)$ ($\vec{T}_g = T_g(t)$) be the vector containing the prior temperature input. A second vector $\vec{P}_T P_T$ with the same number of elements n as $\vec{T}_g T_g$ is generated containing n uniformly distributed random numbers within the limits of an also randomly (equally distributed) chosen standard deviation s . s is chosen from a range of 0.05-0.50 (Fig. ~~A06HS07II~~), which means that the maximum allowed perturbation of a single temperature value $T(t_0)$ is in a range of $\pm 5\%$ to $\pm 50\%$. Creating the synthetic frequencies, $\vec{P}_T P_T$ is low-pass filtered using

Formatiert: Schriftart: Nicht Fett

cubic spline filtering with an equally distributed random ~~cut-off period (cop)~~ (Fig. A064S071) in the range of 500-yr to 2000 yr generating the vector \vec{P} . The new surface temperature input \vec{T}_{sm}^T is calculated from \vec{P} according to:

$$\vec{T}_{sm}^T = \vec{T}_g^T \cdot (\hat{1} + \vec{P}) \quad (8)$$

$$\vec{T}_{sm} = \vec{T}_g^T \cdot (\hat{1} + \vec{P}) \quad (9)$$

The superscript “T” stands for transposed and $\hat{1}$ is the n by 1 matrix of ones.

This approach provides a high potential for parallel computing. In this study, an eight core computer was used, generating and running eight different inputs of \vec{T}_{sm}^T simultaneously, minimizing the time to find an improved solution. For example, during the 706 iterations for the scenario S2, about 5600 different inputs were created and tried, leading to 351 improvements (Tablesee Tab. 01). Since it is possible to find more than one improvement per iteration step due to the parallelization on eight CPU’s, the solution giving the minimal misfit is chosen as new first guess for the next iteration step. This leads to a decrease of the used improvements for the optimization (e.g. for S2, 172 of the 351 improvements were used). Additionally, a first gas age scale is extracted from the model using the last ~~improvement~~ improved conditions, which will then be used in ~~the next step~~ 3.

2.43.3 Adding high frequency information (step 3)

~~Finally, in step 3~~ the missing high frequency temperature ~~information~~ history providing a suitable fit ~~to the between modelled and synthetic~~ $\delta^{15}\text{N}$ ~~target~~ data is directly extracted from the pointwise mismatch $D_{\text{smooth},i}$, between the modelled $\delta^{15}\text{N}_{\text{smooth}}$ ~~signal of the smooth temperature solution given by the Monte Carlo approach obtained in step 2~~ and the synthetic ~~target data~~ $\delta^{15}\text{N}$ target data. Note that for a real reconstruction, this mismatch is calculated using the measured $\delta^{15}\text{N}$ dataset instead of the synthetic one. $D_{\text{smooth},i}$ can be interpreted in first order as the detrended high frequency signal of the synthetic $\delta^{15}\text{N}$ ~~target~~ values (Fig. 04e01c). This signal is transferred to the gas age scale provided by the firm model for the smooth temperature input to ~~reach~~ insure synchronicity in between the ~~gained~~ high frequency temperature variations extracted from the mismatch of $\delta^{15}\text{N}$ on the ice age scale and the smooth temperature solution. Additionally, the signal is shifted by about 10-yr towards modern values to account for ~~the~~ gas diffusion from the surface to the ~~lock in depth~~ LID (Schwander et al., 1993), which is not yet implemented in the firm model. This is necessary for adding the calculated temperature changes (ΔT) to the smooth signal. The ΔT values are calculated according to Eq. (9,10):

$$\Delta T_i = \frac{D_{\text{smooth},i}}{\Omega_{N_2,i}} \quad (9)$$

with the thermal diffusion sensitivity ($\Omega_{N_2,i}$) for the nitrogen isotope fractionation calculated from (Grachev and Severinghaus, 2003; Boersma Klein and De Vries, 1966):

$$\Omega_{N_2,i} = \frac{8.656\text{‰}}{T_i} - \frac{1232\text{‰K}}{T_i^2} \quad (10)$$

$$\Delta T_i = \frac{D_{\text{smooth},i}}{\Omega_{N_2,i}} \quad (10)$$

Formatiert: Schriftart: Nicht Fett

Formatiert: Schriftart: Nicht Fett

Formatiert: Schriftart: Nicht Fett

using the thermal diffusion sensitivity $\Omega_{N_2,i}$ for nitrogen isotope fractionation from Grachev and Severinghaus (2003):

$$\Omega_{N_2,i} = \frac{8.656 \text{ ‰}}{\bar{T}_i} - \frac{1232 \text{ ‰} \cdot \text{K}}{\bar{T}_i^2} \quad (11)$$

\bar{T}_i is the mean firm temperature in Kelvin which is calculated by the firm model for each time point i . To reconstruct the final (high frequency) temperature input T_{hf} , the extracted short term temperature signal ΔT is simply added to the smooth temperature input T_{sm} :

$$T_{hf,i} = T_{sm,i} + \Delta T_i \quad (14)$$

$$T_{hf,i} = T_{sm,i} + \Delta T_i \quad (12)$$

2.4.3.4 Final correction of the surface temperature solution (step 4)

For a further improvement of the remaining $\delta^{15}\text{N}$ and resulting surface temperature misfits, it is important to find a correction method ~~which that~~ contains information ~~which that~~ is also available ~~for measurement when using measured~~ data. The benefit of the synthetic data study is that several later unknown quantities can be calculated, and used for improving the reconstruction approach (see Sect. 3 and 4). For instance, it is possible to split the synthetic $\delta^{15}\text{N}$ data in the gravitational and thermo-diffusion parts or to use the temperature misfit, which is ~~not known later on unknown in reality~~. The idea underlying the correction algorithm explained ~~in the following hereafter~~ is that the remaining misfits of $\delta^{15}\text{N}$ and temperature are connected to the Monte Carlo ~~(step 2)~~ and high frequency part ~~(step 3)~~ of the reconstruction algorithm. ~~In the present inversion framework, it~~ is not possible to find a smooth solution which exactly passes through the $\delta^{15}\text{N}$ target data in the middle of the variance in all parts of the time series. This leads to a slightly over or underestimation of the $\delta^{15}\text{N}$ and their corresponding temperature values. For example, a slightly too low (or too high) smooth temperature estimate leads to a small increase (or decrease) of the firm column height ~~which creates, creating~~ a wrong gravitational background signal in $\delta^{15}\text{N}$ on a later point in time (because the firm column needs some time to react). An additional error in the thermal diffusion signal is also created due to the high frequency part of the reconstruction, because the high frequency information is directly extracted from the deviation of the (synthetic) $\delta^{15}\text{N}$ target data and the modelled $\delta^{15}\text{N}$ data from the smooth solution of the Monte Carlo part. Therefore, this error is transferred into the next step of the reconstruction and partly creates the remaining deviations.

To investigate this problem, the deviations $D_{smooth,i}$ of the synthetic ~~$\delta^{15}\text{N}$~~ -target data ~~$\delta^{15}\text{N}_{target}$~~ to the smooth ~~$\delta^{15}\text{N}$~~ -data ~~$\delta^{15}\text{N}_{smooth}$~~ of the Monte Carlo part is numerically integrated over a time window of 200 yr (see Sect. 4), and thereafter the window is shifted from past to future in 1 yr steps resulting in a time series called IF(t). IF(t) equals a 200 yr running-mean of $D_{smooth,i}$. For t , the mid position of the window is allocated. The time evolution of IF is a measure for the deviation of the smooth solution in $\delta^{15}\text{N}$ (or temperature) from the perfect middle passage through the target data and for the slightly over and underestimation of the resulting temperature.

$$IF(t_i) = \int_{t_i-100}^{t_i+100} (\delta^{15}N_{syn,meas}(t) - \delta^{15}N_{smooth}(t)) dt \quad (12)$$

with $t_i = t_x + \frac{t_2 - t_1}{2}$ ~~IF(t_i) = ∫_{t₁}^{t₂} (δ¹⁵N_{target}(t) - δ¹⁵N_{smooth}(t)) dt~~

$$(13)$$

where $t_i = t_1 + \frac{t_2 - t_1}{2}$ ~~(14)~~

Next, the sample cross correlation function (xcf) (Box et al., 1994) is applied to IF(t) and the remaining misfits $D_{\delta^{15}N, hf}$ of $\delta^{15}N$ after the high frequency part. The xcf shows two extrema (Fig. 05a02a), a maximum (xcf_{max}) and a minimum (xcf_{min}) at two certain lags (lag_{max, D $\delta^{15}N$} at xcf_{max} and lag_{min, D $\delta^{15}N$} at xcf_{min}). Now, the same analysis is conducted for IF(t) versus the temperature mismatch $D_{T, hf}$ (Fig. 05b02b), which shows an equal behaviour (two extrema, lag_{max, T} at xcf_{max} and lag_{min, T} at xcf_{min}). Comparing the two cross correlations shows that lag_{max, D $\delta^{15}N$} ~~—equals the negative~~ lag_{min, T} and lag_{min, D $\delta^{15}N$} ~~—corresponds to the negative~~ lag_{max, T} (Fig. 05d02d,e). The idea for the correction is that the extrema in $D_{\delta^{15}N, hf}$ with the positive lag (positive means here that $D_{\delta^{15}N, hf}$ has to be shifted to past values relative to IF) creates the misfit of temperature $D_{T, hf}$ on the negative lag (modern direction) and vice versa. So IF(t) yields information about the cause and ~~gives a handle for~~ ~~correcting allows us to correct~~ this effect between the remaining mismatches of $\delta^{15}N$ and temperature over the whole time series. The lags are not sharp signals, ~~which results from due to the easefact~~ that (i) the cross correlations are conducted over the whole analysed record, ~~which leads leading~~ to an averaging of this cause and effect relationship as well as that (ii) IF(t) is a smoothed quantity itself. The correction of the reconstructed temperature after the high frequency part is conducted in the following way: From the two linear relationships between IF(t) and $D_{\delta^{15}N, hf}$ at the two lags (lag_{max, D $\delta^{15}N$} at xcf_{max}, lag_{min, D $\delta^{15}N$} at xcf_{min}) two sets of $\delta^{15}N$ correction values ($\Delta\delta^{15}N_{max}$ from xcf_{max} and $\Delta\delta^{15}N_{min}$ from xcf_{min}) are calculated. ~~Now Then~~ the lags are being inverted (Fig. 05e02c,e) shifting the two sets of the $\delta^{15}N$ correction values to the attributed lags of the cross correlation between IF(t) and $D_{T, hf}$ (e.g. $\Delta\delta^{15}N_{min}$ to lag from xcf_{max} from the cross correlation between IF(t) and $D_{T, hf}$) ~~therefore~~ changing the time assignments of $\Delta\delta^{15}N_{min}(t)$ and $\Delta\delta^{15}N_{max}(t)$ to $\Delta\delta^{15}N_{min}(t + lag_{max, T})$ and $\Delta\delta^{15}N_{max}(t + lag_{min, T})$. Now, the $\Delta\delta^{15}N_{max}$ and $\Delta\delta^{15}N_{min}$ are component wise summed up leading to the time series $\Delta\delta^{15}N_{cv}(t)$. From Eq. ~~(9)~~ (10) with $\Delta\delta^{15}N_{cv,i}$ instead of $D_{smooth,i}$ the corresponding temperature correction values are calculated and added to the high frequency temperature solution giving the corrected temperature T_{corr} . Finally, T_{corr} is used to run the firm model to calculate the corrected $\delta^{15}N$ time series (Fig. 0603). This cause and effect relationship found in the cross correlations between IF(t) and $D_{\delta^{15}N, hf}$, and IF(t) and $D_{T, hf}$, is exemplarily shown in Fig. 0502 for ~~the~~ scenario S1 and was found for all eight synthetic scenarios. The derived correction algorithm leads to a further reduction of the mismatches of about 40 % in $\delta^{15}N$ and temperature (see Sect. 3.2).

3. Results

3.1 Monte Carlo type input generator

Figure A07S08 shows the evolution of the mean misfit D_{mean} of $\delta^{15}N$ ~~offrom~~ the synthetic target versus the modelled data as a function of the applied iterations for all synthetic scenarios. One can easily see that ~~for~~ all scenarios, ~~there is show~~ a steep

decline of the mismatch during the first 50- to 200 iterations followed by a rather moderate decrease, and which finally leads to a constant value. During the Monte Carlo part, it was possible to reduce the misfit of $\delta^{15}\text{N}$ compared to the first guess solution by about 15 % to 75 % depending on the scenario and the mismatch of the first guess solution (Table see Tab. 01). This leads to a reduction of the temperature mismatches compared to the first guess temperature mismatch of about 51 % to 87 %.

Figure 01 provides the comparison between the first guess and Monte Carlo solution versus the synthetic target data for the modelled $\delta^{15}\text{N}$ (a-c) and surface temperature values (d-f) for the scenario scenario S5. Subplots (a) and (d) show the time series of the synthetic target data (black dotted line), the first guess solution (blue line) and the Monte Carlo solution (red line) for $\delta^{15}\text{N}$ and temperature. In subplots (b) and (e), the distribution of the pointwise mismatch D_i of the first guess (blue) and the Monte Carlo solution (red) versus the synthetic target data for $\delta^{15}\text{N}$ and temperature can be found. Subplots (c) and (f) contain the time series for D_i for $\delta^{15}\text{N}$ and temperature. The $D_i(\delta^{15}\text{N})$ data is used later on to calculate the high frequency signal that is superimposed to the smooth temperature solution according to Eq. (9) (10) and Eq. (11) (12) (see Sect. 2.43.3). From Fig. 0401 it can be concluded that the Monte Carlo part of the reconstruction algorithm (step 2) leads to two major improvements of the first guess solution. First, it is obvious that the Monte Carlo approach corrects the offsets of the first guess input, which shifts the midpoint of the distribution of D_i to zero (see Fig. 0401b,e). The second improvement is that the distribution becomes more symmetric and the misfit is overall reduced (the distributions become narrower) compared to the first guess, due to the middle passage through the $\delta^{15}\text{N}$ targets. These improvements can be observed for all eight synthetic scenarios, showing the robustness of the Monte Carlo part (Table see Tab. 01, Fig. 04, and Fig. S03-S0901).

3.2 High frequency step and final correction

Figure 03 provides the comparison between the Monte Carlo, the high frequency and the correction parts of the reconstruction procedure for the scenarios S5. Additional data and corresponding plots for all other scenarios can be found in Table table 02 and Fig. S10-S16. The upper four plots (a-d) illustrate each reconstruction step and their effect on the modelled $\delta^{15}\text{N}$; the bottom four plots (e-h) show the corresponding results on the temperature. Plots (a) and (d) contain the time series of the synthetic $\delta^{15}\text{N}$ or temperature target (black dotted line), the high frequency solution (blue line), and the final solution after the correction part (red line). For visibility reasons, subplots (b) and (f) display a zoom-in for a randomly chosen time window of about 500 yr for the same quantities, which shows the excellent agreement in timing and amplitudes of the modelled $\delta^{15}\text{N}$ and temperature compared to the synthetic target data. Histograms (c) and (g) and subplots (d) and (h) show the distribution and the time series of the pointwise mismatches D_i (D_i for $\delta^{15}\text{N}$, ΔT_i for temperature) between the modelled and the synthetic target data in $\delta^{15}\text{N}$ and temperature for each reconstruction step.

Compared to the Monte Carlo solution, the high frequency part leads to a large refinement of the reconstructions. For the mean $\delta^{15}\text{N}$ misfits D , the improvement between the Monte Carlo and the high frequency parts is in the range of 64 % to 76 % (see Table Tab. 02). This leads to a reduction of the temperature mismatches of 43 % to 67 %. The standard deviations

(1 σ) of the pointwise mismatches (Fig. [06e03c,d,g,h](#)) in $\delta^{15}\text{N}$ and temperature after the high frequency parts are in the range of about 2.7 permeg to 5.4 permeg for $\delta^{15}\text{N}$ and 0.22 K to 0.40 K for the reconstructed temperatures depending on the scenario, which is clearly visible in the decreasing width of the histograms (subplots (c) and (g) of Fig. [0603](#), blue against grey).

5 The mismatches after the correction part of the reconstruction approach show clearly a further decrease of the misfits. This means that the width of the distributions of the pointwise mismatches of $\delta^{15}\text{N}$ as well as of temperature is further reduced, and the distributions become more symmetric (long tails disappear, see histogram (c) and (g) of Fig. [0603](#)). The time series of the mismatches (subplots (d) and (h) of Fig. [0603](#)) clearly illustrate that the correction approach mainly tackles the extreme deviations (sharp reduction of extreme values occurrence in the red distribution compared to the blue distribution) leading to a further improvement of about 40-% in $\delta^{15}\text{N}$ and temperature. Finally, the 95-% quantiles of the remaining pointwise mismatches of $\delta^{15}\text{N}$ and temperature (D_i or ΔT_i) were calculated for the final solutions for all scenarios and are used as an estimate for the 2σ uncertainty of the reconstruction algorithm (see Fig. [06, Fig. S10-S16,03](#) and [Table Tab. 2](#)). The final uncertainties (2σ) are in the order of 3.0 permeg to 6.3 permeg for $\delta^{15}\text{N}$ and 0.23 K to 0.51 K for the surface temperature misfits. It is noteworthy that the measurement uncertainties (per point) of state of the art $\delta^{15}\text{N}$ measurements are
15 in the same order of magnitude, i.e. 3- permeg to 5 permeg (Kobashi et al., 2008), highlighting the effectiveness of the presented fitting approach (Kobashi et al., 2008b), highlighting the effectiveness of the presented fitting approach. Table 03 contains the final mismatches (2σ) in Δ age between the synthetic target and the final modelled data after the correction step for all scenarios and shows that with a known accumulation rate and assumed perfect firm physics, it is possible to fit the Δ age history in the Holocene with mean uncertainties better than 2 yr. In other words, the uncertainty in Δ age reconstruction due to the inversion algorithm alone is in the order of 2 yr.
20

4. Discussion

4.1 Monte Carlo type input generator

Figure [A06S07](#) shows the distribution of the ~~cut-off periods (cop)~~ (I-) and ~~the distribution of the~~ s values (II) used to create the improvements (~~see methods-Sect. 2.43.2~~) for all scenarios. The cop values are more or less evenly distributed, which
25 shows that nearly the whole of the allowed frequency range (allowed cops were 500 yr to 2000 yr) was used to create the improvements during the iterations. In contrast, the distributions of the s values show clearly that mostly small s values are used to create the improvements, which implies that ~~during the iterations~~ with small perturbations ~~are~~ more likely lead to an improvement than larger ones.

~~Yet, Fig. A07Figure S08~~ reveals a weak spotpoint of the Monte Carlo part, namely the absence of a suitable termination criterion for the optimization. The implementation until now is conducted such that the maximum number of iterations is
30 given by the user or the iterations are terminated after a certain time (e.g. 15 h). Figure [A07S08](#) shows that for nearly all scenarios it would be possible to stop the optimization after about 400 iterations, due to rather small additional

improvements later on. This would decrease the ~~amount of~~ time needed for the Monte Carlo part to about 10 h (a single iteration needs about 90 s). Since the goal of the Monte Carlo part is to find a temperature realisation that leads to an optimal middle passage through the $\delta^{15}\text{N}$ target data, it would be possible to use the mean difference between the $\delta^{15}\text{N}$ target and spline filtered $\delta^{15}\text{N}$ data using a certain cut off period as a termination criterion. This issue is under investigation at the moment. Another possibility to decrease the time needed for the Monte Carlo part could be an increase in the numbers of CPUs used for the parallelization of the model runs. For this study an eight core parallelization was used. A further increase in numbers of workers would improve the speed of the optimization.

4.2 High frequency step and final correction

~~In several analyses were conducted in~~ order to investigate the remaining mismatches in $\delta^{15}\text{N}$ and temperature after the high frequency and the correction part of the reconstruction, ~~several analyses were conducted, respectively.~~ First, the total misfit of $\delta^{15}\text{N}$ ($D_{\delta^{15}\text{N}_{\text{tot}}}$) was separated into two fractions: gravitational ($D_{\delta^{15}\text{N}_{\text{grav}}}$) and thermal diffusion mismatches ($D_{\delta^{15}\text{N}_{\text{therm}}}$) of $\delta^{15}\text{N}$ (Fig. 0704). Figure 0704 indicates that the main fraction of the total mismatch of $\delta^{15}\text{N}$ is due to the misfit of the thermal diffusion component of the $\delta^{15}\text{N}$ signal, whereas the gravitational misfit of $\delta^{15}\text{N}$ has only a minor contribution. The ratio of the standard deviations $\sigma(D_{\delta^{15}\text{N}_{\text{therm}}})/\sigma(D_{\delta^{15}\text{N}_{\text{grav}}})$ is about 2.4 for the high frequency solution, and about 2.3 for the corrected signal, showing that the misfit in the thermal diffusion part is more than twice as high as in the gravitational component.

To investigate the timing and contributions of the mismatches in $\delta^{15}\text{N}$ and temperature for scenario S1, different xcfs were calculated (Fig. A08aS09a-d). The same analyses were conducted for all synthetic scenarios, leading to similar results. In Fig. A08aS09a the xcf between the mismatch of total $\delta^{15}\text{N}$ ($D_{\delta^{15}\text{N}_{\text{tot},\text{hf}}}$) and the misfit of temperature ($D_{T,\text{hf}}$) is shown. The cross correlation leads to two extrema ($r_{1a}=0.70$, $r_{2a}=-0.55$) on two certain lags ($l_{1a}=-2$ yr, $l_{2a}=+126$ yr). In subplot (b) and (c) the same analysis is conducted between the mismatch of the gravitational ($D_{\delta^{15}\text{N}_{\text{grav},\text{hf}}}$) component (b), and the thermal diffusion ($D_{\delta^{15}\text{N}_{\text{therm},\text{hf}}}$) component (c) of $\delta^{15}\text{N}$ and the temperature mismatch. It is obvious that the xcf of (a) is a combination of (b) and (c). The direct correlation on l_{1a} of (a) can be attributed mainly to the mismatch of the thermal diffusion component of $\delta^{15}\text{N}$, whereas the negative correlation on l_{2a} is due to the mismatch of the gravitational component of $\delta^{15}\text{N}$. Regarding the xcfs of (a)-(c) at a certain lag l , i.e. $l = 0$ yr shows that here (and on most of the other lags) the correlations between $D_{\delta^{15}\text{N}_{\text{grav},\text{hf}}}$ with $D_{T,\text{hf}}$ and $D_{\delta^{15}\text{N}_{\text{therm},\text{hf}}}$ with $D_{T,\text{hf}}$ work in opposite directions, which makes it difficult to find a way to correct the remaining temperature mismatch using only information from $D_{\delta^{15}\text{N}_{\text{tot},\text{hf}}}$ for measurement data (where when only $D_{\delta^{15}\text{N}_{\text{tot},\text{hf}}}$ is available). The correlation on l_{1a} in (a) is weakened, whereas the lag l_{2a} is shifted to higher values because of the superposition of gravitational and thermal diffusion mismatch. Figure A08dS09d shows also that the gravitational and thermal diffusion mismatches of $\delta^{15}\text{N}$ are not independent, but the correlations at the extrema are relatively weak ($r_{1d}=0.38$, $r_{2d}=-0.56$). The negative correlation r_{2d} is a sign for the compensation effect between the gravitational and thermal diffusion signals in $\delta^{15}\text{N}$ due to the high frequency part of the reconstruction, whereas no explanation could be found for the positive correlation r_{1d} . The symmetric behaviour of the lags for r_{1d} and r_{2d} ($l_{1d} = -88$ yr $\approx -l_{2d} = 93$ yr) suggest that r_{1d} could be an artefact of a periodic behaviour of $D_{\delta^{15}\text{N}_{\text{grav},\text{hf}}}$ and $D_{\delta^{15}\text{N}_{\text{therm},\text{hf}}}$. Figure A09aFigures S10a-d show the same analysis after the

correction part of the reconstruction. It is evident that in all cases the extrema in the different xcfs break down due to the correction of the temperature signal, which is the consequence of the decreasing mismatches of temperature as well as of $\delta^{15}\text{N}$. The comparison of the subplots (a), (b) and (c) also shows that the remaining temperature misfits after the correction are mainly driven by the mismatches of the thermal diffusion signal of $\delta^{15}\text{N}$ with a minor contribution of the gravitational misfit.

Figures A08S09e-h show the cross correlations between IF(t) used for the correction of the high frequency temperature solution, and the temperature misfit (e), the mismatch of total $\delta^{15}\text{N}$ (f), the mismatch of the gravitational (g) and thermal diffusion (h) component of the $\delta^{15}\text{N}$ signal calculated from the high frequency temperature solution. For the correction, the cross correlations (e) and (f) were used (see Sect. 2.43.4 and Fig. 0502). Since for ~~measurement~~measured data neither information about the temperature mismatch (the true temperature is not known) nor about the mismatch of the components of $\delta^{15}\text{N}$ (gravitational, thermal diffusion) are available, it is imperative that the symmetric behaviour between the xcf(IF(t), $D_{\delta^{15}\text{Ntot,hf}}$) and inverted xcf(IF(t), $D_{\delta^{15}\text{Ntot,hf}}$) holds true. This criterion is fulfilled for all eight synthetic data scenarios and especially for H1-H3. The comparison of the subplots (f), (g) and (h) of Fig. A08S09 show the same findings as before, namely that the xcf for IF versus $D_{\delta^{15}\text{Ntot,hf}}$ is the combination of the xcfs of IF(t) versus $D_{\delta^{15}\text{Ngrav,hf}}$ and IF(t) versus $D_{\delta^{15}\text{Ntherm,hf}}$ and that the major fraction of $D_{\delta^{15}\text{Ntot,hf}}$ is contributed from $D_{\delta^{15}\text{Ntherm,hf}}$. The advantage to use IF(t) for the correction is the symmetry between the two cross correlations, which is created by two factors. The first one is the allocation of the window mid position to the entries of IF, which leads to the symmetric behaviour of the gravitational and thermal diffusion misfits. Second, the shifting of the window in 1 yr steps creating IF(t) over the whole data set leads to an averaged information, but even more importantly, to constant ~~dependene~~dependency between the temperature and $\delta^{15}\text{N}$ mismatches. This can be used later on to fit ~~measurement~~measured data.

Additionally, the influence of the window length, used for the construction of IF(t), on the correction was analysed. The construction was conducted for different window lengths ranging from 50 yr to 750 yr (Fig. A10S11). Also, the correction was calculated by using only xcf_{max} or xcf_{min} of IF(t) versus $D_{\delta^{15}\text{N,hf}}$ for correcting the temperature input. Figures A10aS11a,b show the remaining mismatches of $\delta^{15}\text{N}$ ($D_{\delta^{15}\text{N,corr}}$) (a), and temperature ($D_{\text{T,corr}}$) (b) after the correction as a function of the used window length for IF(t). The analysis shows that for all investigated window lengths the correction reduces the mismatches of $\delta^{15}\text{N}$ and temperature, whatever correction mode was used (calculated with xcf_{max} , xcf_{min} , or both quantities, see comparison with the blue line in (a) and (b)). Furthermore, the correction works best for window lengths in the range of 100 yr to 300 yr with an optimum at 200 yr for all cases. This indicates that the maximum mean duration effect of a $\delta^{15}\text{N}$ mismatch creating a temperature mismatch (and vice versa) is in the same range for the investigated scenarios and such small deviations (low permeg level). It is also visible that the correction using both extrema (xcf_{max} and xcf_{min}) leads to a better correction as the approach using only one quantity. This is somehow surprising because the two extrema are the result of the periodicity of IF(t), $D_{\delta^{15}\text{N,hf}}$ and $D_{\text{T,hf}}$. ~~One An~~ explanation for ~~thatthis~~ result could be that a larger section of the temperature time series is corrected when both extrema are used for the correction, due to ~~shifting~~shifts in both directions. The correction using xcf_{max} only leads to a better fit than the one with xcf_{min} , which can be attributed to the higher correlation

between IF(t) and $D_{\delta^{15}\text{N},\text{HF}}$. Figures A10eS11e,f show the evolution of the lags corresponding to the two extrema for the cross correlations between IF(t), and the $\delta^{15}\text{N}$ and temperature mismatches, respectively. The linear dependency between the lags and the window length (the lags are nearly half of the window length) is the result of the construction of IF(t), which means the averaging due to the integration in the window of this certain length and the symmetric behaviour due to the allocation of the window mid position to the entries of IF(t).

4.3 Key points to be considered for the application to real data

Benefits of the novel gas isotope fitting approach

In addition to the fitting of $\delta^{15}\text{N}$ data, the algorithm is able to fit $\delta^{40}\text{Ar}$ and $\delta^{15}\text{N}_{\text{excess}}$ data as well using the same basic concepts (Fig. S12). Here the $\delta^{40}\text{Ar}$ and $\delta^{15}\text{N}_{\text{excess}}$ data from Kobashi et al. (2008) were used as the fitting targets using the same approach. We reach final mismatches (2σ) of 4.0 permeg for $\delta^{40}\text{Ar}/4$ and 3.7 permeg for $\delta^{15}\text{N}_{\text{excess}}$, which are for both quantities below the analytical measurement uncertainty of 4.0 permeg to 9.0 permeg for $\delta^{40}\text{Ar}/4$ and 5.0 permeg to 9.8 permeg for $\delta^{15}\text{N}_{\text{excess}}$ measured data (Kobashi et al., 2008).

The automated inversion of different gas isotope quantities ($\delta^{15}\text{N}$, $\delta^{40}\text{Ar}$, $\delta^{15}\text{N}_{\text{excess}}$) provides a unique opportunity to study the differences in the gained solutions using different targets and to improve our knowledge about the uncertainties of gas isotope based temperature reconstructions using a single firm model. Next, the presented algorithm is not dependent on the firm model, which leads to the implication that the algorithm can be coupled to different firm models describing firm physics in different ways. Furthermore, an automated reconstruction algorithm avoiding manual manipulation and leading to reproducible solutions makes it possible for the first time, to study and learn from the differences in between solutions matching different targets. Finally, differences obtained by applying different firm physics (densification equations, convective zone, etc.) but the very same inversion algorithm may help to assess firm model shortcomings, resulting in more robust uncertainty estimates than it was ever possible before.

In this publication we show the functionality and the basic concepts of the automated inversion algorithm using well known synthetic $\delta^{15}\text{N}$ fitting targets. In this “perfect world scenario” the forward problem, converting surface temperature to $\delta^{15}\text{N}$, as well as the inverse problem, converting $\delta^{15}\text{N}$ to surface temperature, is completely described by the used firm model. Consequently all sources of signal noise are ignored. For the later use of the algorithm on $\delta^{15}\text{N}$, $\delta^{40}\text{Ar}$ or $\delta^{15}\text{N}_{\text{excess}}$ measured data this will not be the case anymore due to different sources of signal noise in the used measured data. As a result, differences in between temperature solutions obtained from individual targets ($\delta^{15}\text{N}$, $\delta^{40}\text{Ar}$, $\delta^{15}\text{N}_{\text{excess}}$) will become obvious. These differences will allow to quantify the uncertainties associated with different unconstrained processes. Next, we will list and discuss potential sources of uncertainties and try to provide suggestions for their handling and quantification in our approach.

Measurement uncertainty and firm heterogeneity (cm-scale variability):

5 Many studies have investigated the influence of firm heterogeneity (or density fluctuations) on measurements of air compounds and quantities (e.g. $\delta^{15}\text{N}$, $\delta^{40}\text{Ar}$, CH_4 , CO_2 , O_2/N_2 ratio, air content) extracted from ice cores resulting in cm-scale variability and leading to additional noise on the measured data (e.g., Etheridge et al., 1992; Huber and Leuenberger, 2004; Fujita et al., 2009; Capron et al., 2010; Hörhold et al., 2011; Rhodes et al., 2013, 2016; Fourteau et al., 2017). Using discrete measurement technique instead of continuous sampling methods makes it difficult to quantify these effects. However, during discrete analyses of ice core air data it is common to measure replicates for given depths, from which the measurement uncertainties of the gas isotope data is calculated using pooled-standard-deviation (Hedges L. V., 1985). Often it is not possible to take real replicates (same depth) and instead the replicates are taken from nearby depths. Hence, any potential cm-scale variability is to some degree already included in the measurement uncertainty, because each measurement point represents the average over a few centimetres of ice. This is especially the case for low accumulation sites or glacial ice samples for which the vertical length of a sample (e.g., 10-25 cm long for the glacial part of the NGRIP ice core, Kindler et al., 2014) covers the equivalent of 20 yr to 50 yr of ice at approximately 35 kyr b2k. Increasing the depth resolution of the samples would increase our knowledge of cm-scale variability, for e.g. identifying anomalous entrapped gas layers that could have been rapidly isolated from the surface due to an overlying high density layer (e.g., Rosen et al., 2014). As this variability is likely due to heterogeneity in the density profile, modelling such heterogeneities (if possible at all) may not help to better reconstruct a meaningful temperature history, but rather to reproduce the source of noise. This means that the potential cm-scale variability, in many cases, is already incorporated in the analytical noise obtained from gas isotope measurements, due to analytical techniques themselves. Assuming the measurement uncertainty as Gaussian distributed, it is easy to incorporate this source of uncertainty in the inverse modelling approach presented here. This will increase the uncertainty of the temperature according to Eq.(10).The same equation can also be used for the calculation of the uncertainty in temperature related to measurement uncertainty in general.

10
15
20
25 To answer the pertinent question of how to better extract a meaningful temperature history from a noisy ice core record, an excellent – but costly – solution is of course to use multiple ice cores. For example, a $\delta^{15}\text{N}$ -based temperature reconstruction from the combination of data from the GISP2 ice core with the “sister ice core” GRIP drilled only a few kilometres apart is likely one of the best ways to overcome potential cm-scale variability. A comparison of ice cores that were drilled even closer might be even more advantageous.

Smoothing effects due to gas diffusion and trapping:

30 It is known that gas diffusion and trapping processes in the firm can smooth out fast signals and result in a damping of the amplitudes of gas isotope signals (e.g. Spahni et al., 2003; Grachev and Severinghaus, 2005). The duration of gas diffusion from the top of the diffusive column to the bottom where the air is closed off in bubbles is for Holocene conditions in Greenland approximately in the order of 10 yr (Schwander et al. 1997), whereas the data resolution of the synthetic targets was set to 20 yr to mimic the measurement data from Kobashi et al. (2008) with a mean data resolution of about 17 yr (see Sect. 2.3: “Generating synthetic target data”). In the study of Kindler et al. (2014) it was shown that a glacial Greenland LID

leads to a damping of the $\delta^{15}\text{N}$ signal of about 30 % for a 10 K temperature rise in 20 yr. We further assume that the smoothing according to the lock-in process is negligible for Greenland Holocene conditions according to the much smaller amplitude signals and shallower LID. Yet, for glacial conditions it requires attention.

Accumulation rate uncertainties:

For the synthetic data study presented in this paper it is assumed that the used accumulation rate data is well known with zero uncertainty. This simplification is used to show the functionality and basic concepts of the presented fitting algorithm in every detail on well-known $\delta^{15}\text{N}$ and temperature targets and to focus on the final uncertainties originating from the presented fitting algorithm itself. For the later reconstruction using measured gas isotope data together with the published accumulation rate scenarios shown in Fig. S01 this will not be the case anymore. Uncertainties in layer counting and corrections for ice thinning lead to a fundamental uncertainty. Especially in the early Holocene, this can easily exceed 10 %. As the accumulation rate data is used to run the firm model, all potential accumulation uncertainties are in part incorporated into the temperature reconstruction. On the other hand, as we discussed in section 2.3, the accumulation rate variability has a minor impact compared to the input temperature on the variability of $\delta^{15}\text{N}$ data in the Holocene (see also Fig. S03, Fig. S04). The influence of these quantities, accumulation rate or temperature, on the temperature reconstruction is not equal; during the Holocene, accumulation rate variability explains about 12 % to 30 % of $\delta^{15}\text{N}$ variability. 30 % corresponds to the 8.2 kyr event and 12 % for the mean of the whole Holocene period including the 8.2 kyr event. Hence the influence of accumulation changes, excluding the extreme 8.2 kyr event, is generally below 10 % during the Holocene. If the accumulation is assumed to be completely correct then the missing part will be assigned to temperature variations. Nevertheless for the fitting of the Holocene measurement data we will use all three accumulation rate scenarios as shown in Fig. S01. The difference in the reconstructed temperatures arising from the differences of these three scenarios will be used for the uncertainty calculation as well and is most likely higher than the uncertainty arising from uncertainties due to the process of producing the accumulation rate data and from the conversion of the accumulation rate data to the GICC05 timescale.

Convective zone variability:

Many studies have shown the existence of a non-diffusive zone at the top of the diffusive firm column, called convective zone (CZ). The CZ is formed by strong katabatic winds and pressure gradients between the surface and the firm (e.g. Kawamura et al., 2006, 2013; Severinghaus et al., 2010). The existence of a CZ changes the gravitational background signal in $\delta^{15}\text{N}$ and $\delta^{40}\text{Ar}$ as it reduces the diffusive column height. The presented fitting algorithm was used together with the two most frequently used firm models for temperature reconstructions based on stable isotopes of air, the Schwander et al. (1997) model which has no CZ build in (or better a constant CZ of 0 m) and the Goujon firm model (Goujon et al., 2003) (which assumes a constant convective zone over time, that can easily be set in the code). This difference between the two firm models only changes significantly the absolute temperature rather than the temperature anomalies as it was shown by other studies (e.g., Guillevic et al., 2013, Fig. 3). In the presented work, we show the results using the model from Schwander et al.

(1997), because the differences between the obtained solutions using the two models are negligible besides a constant temperature offset. Also, noteworthy is that there is no firm model at the moment which uses a dynamically changing CZ. Indeed, this should be investigated but requires additional intense work. Additionally, the knowledge of the time evolution of CZ changes for time periods of millennia to several hundreds of millennia (in frequency and magnitude) is too poor to estimate the influence of this quantity on the reconstruction. In principle it is possible to cancel out the influence of a potentially changing CZ by using $\delta^{15}\text{N}_{\text{excess}}$ data for temperature reconstruction, as due to the subtraction of $\delta^{40}\text{Ar}/4$ from $\delta^{15}\text{N}$ the gravitational term of the signals is eliminated. From that point of view it will be interesting to compare temperature solutions gained from $\delta^{15}\text{N}_{\text{excess}}$ fitting with the solutions based on $\delta^{15}\text{N}$ or $\delta^{40}\text{Ar}$ alone. This can offer a useful tool for quantifying the magnitude and frequency of CZ changes in the time interval of interest.

It is known that for some very low accumulation rate sites in areas with strong katabatic winds (e.g. “Megadunes”, Antarctica) extremely deep CZs can occur, which are potentially able to smooth out even decadal-scale temperature variations (Severinghaus et al., 2010). For this its deepness would need to be of several dozens of meters, which is highly unrealistic even for glacial Summit conditions (Guillevic et al., 2013, see discussion in Annex A4, p. 1042) as well as for the rather stable Holocene period in Greenland for which no low accumulation and strong katabatic wind situations are to be expected.

4.4 Proof of concept for glacial data

For glacial conditions the task of reconstructing temperature (with correct frequency and magnitude) without using $\delta^{18}\text{O}_{\text{ice}}$ information is much more challenging due to the highly variable gas age - ice age differences (Δage) between stadial and interstadial conditions. Here, contrary to the rather stable Holocene period, the Δage can vary by several hundreds of years. Also the accumulation rate data is more uncertain than for the Holocene. To prove that the presented fitting algorithm also works for glacial conditions we inverted the $\delta^{15}\text{N}$ data measured for the NGRIP ice core by Kindler et al. (2014) for two Dansgaard-Oeschger events, namely DO6 and DO7. Since the magnitudes of those events are higher and the signals are smoother than in the Holocene we only had to use the Monte Carlo type input generator (see Sect. 2.3.2) for changing the temperature inputs. To compare our results to the $\delta^{18}\text{O}_{\text{ice}}$ -based and manually calibrated values from Kindler et al. (2014) we use the ss09sea06bm time scale (NGRIP members: Andersen et al., 2004; Johnsen et al., 2001) as it was done in the Kindler et al. publication. For the model spin-up we use the accumulation rate and temperature data from Kindler et al. (2014) for the time span 36.2 kyr to 60 kyr. The reconstruction window (containing DO6 and DO7) is set to 32 kyr to 36.2 kyr. As the first guess (starting point) of the reconstruction we use the accumulation rate data for NGRIP from the ss09sea06bm time scale together with a constant temperature of about $-49\text{ }^{\circ}\text{C}$ for this time window. As minimization criterion D for the reconstruction we simply use the sum of the mean squared errors of the $\delta^{15}\text{N}$ and Δage mismatches weighted with their uncertainties (wRMSE) according to the following equation instead of the mean $\delta^{15}\text{N}$ misfit alone as used for the Holocene (Eq. (8)).

$$D = \sqrt{\text{wRMSE}(\delta^{15}\text{N})} + \sqrt{\text{wRMSE}(\Delta\text{Age})} \quad (15)$$

$$= \sqrt{\frac{1}{N} \sum_i \left[\frac{\delta^{15}\text{N}_{\text{meas},i} - \delta^{15}\text{N}_{\text{mod},i}}{\varepsilon_{\delta^{15}\text{N},i}} \right]^2} + \sqrt{\frac{1}{M} \sum_j \left[\frac{\Delta\text{Age}_{\text{meas},j} - \Delta\text{Age}_{\text{mod},j}}{\varepsilon_{\Delta\text{Age},j}} \right]^2}$$

Here $\varepsilon_{\delta^{15}\text{N},i}$ and $\varepsilon_{\Delta\text{Age},j}$ are the uncertainties in $\delta^{15}\text{N}$ and ΔAge for the measured values i or j (ΔAge match points: Guillevic, M. (2013), p.65, Tab. 3.2) and N, M the number of measurement values. We set $\varepsilon_{\delta^{15}\text{N},i} = 20$ permeg for all i (Kindler et al., 2014) and $\varepsilon_{\Delta\text{Age},j} = 50$ yr for all j . The relative uncertainties in ΔAge can easily reach up to 50 % and more in the Glacial using the ss09sea06bm time scale which results in a pre-eminence of the $\delta^{15}\text{N}$ misfits over the ΔAge misfits (10 % to 20 % when using GICC05 time scale, Guillevic (2013), p. 65 Tab. 3.2). Due to this issue we have to set ΔAge uncertainties to 50 yr to make both terms equally important for the fitting algorithm. In Fig. S13 we show preliminary results. The $\delta^{15}\text{N}$ and ΔAge fitting (a, b) and the resulting gained temperature and accumulation rate solutions (c, d) using the presented algorithm are completely independent from $\delta^{18}\text{O}_{\text{ice}}$ which provides the opportunity to evaluate the $\delta^{18}\text{O}_{\text{ice}}$ based reconstructions. In this study the algorithm was used in three steps. First, starting with the first guess (constant temperature), the temperature was changed as explained before. The accumulation rate was changed in parallel to the temperature allowing a random offset shift (up and down) together with a stretching or compressing (in y direction) of the accumulation rate signal over the whole time window (32 kyr to 36.2 kyr). This first step leads to the “Monte Carlo Solution 0” (MCS0) which provides a first approximation and is the base for the next step. For the next step, we fixed the accumulation rate and let the algorithm only change the temperature to improve the $\delta^{15}\text{N}$ fit (MSC1). Finally, we allow the algorithm to change the temperature together with the accumulation rate using the Monte Carlo type input generator for both quantities. This allows to change the shape of the accumulation rate data. This final step can be seen as a fine tuning of the gained solutions from the steps before. The obtained mismatches in $\delta^{15}\text{N}$ and ΔAge of all steps are at least of the same quality or better than the $\delta^{18}\text{O}_{\text{ice}}$ based manual method from Kindler et al. (2014) (see Tab. S02). The gained temperature solutions show a very good agreement in timing and magnitude compared to the reconstruction of Kindler et al. (2014). Also the accumulation rate solutions show that the accumulation has to be reduced significantly compared to the ss09sea06bm data to allow a high quality fit of the $\delta^{15}\text{N}$ and ΔAge target data, a result highly similar to Guillevic et al. (2013) and Kindler et al. (2014). The mismatches in $\delta^{15}\text{N}$ and ΔAge of the final MCS FIN solution show a 15 % smaller misfit in $\delta^{15}\text{N}$ (2σ) and an about 31 % smaller misfit for ΔAge (2σ) compared to the Kindler et al. (2014) solution. Keeping in mind that the used approach is completely independent from $\delta^{18}\text{O}_{\text{ice}}$ strengthens the functionality and quality of the presented gas isotope fitting approach also for glacial reconstructions. As this section contains a proof of concept of the presented automated gas isotope fitting algorithm on glacial data, preliminary results and ongoing work were shown here. Furthermore as the presented fitting algorithm was developed and tested in first order for Holocene like data, it is highly probable that the functionality of the algorithm using glacial data will be further extended and adjusted in future studies.

5. Conclusion

A novel approach is introduced and described for inverting a firn densification and heat diffusion model to fit small gas isotope data variations as observed throughout the Holocene. From this new fitting method, it is possible to extract the surface temperature history that drives the firn status which in turn leads to the gas isotope time series. The approach is a combination of a Monte Carlo ~~sampling based iterative method~~ and ~~quantitative data~~ analysis ~~of remaining mismatches between modelled and target data~~. The procedure works fully automated and provides a high potential for parallel computing for time consumption optimization. Additional sensitivity experiments have shown that accumulation rate changes have only a minor influence on short term variations of $\delta^{15}\text{N}$, which themselves are mainly driven by high frequency temperature variations. To evaluate the performances of the presented approach, eight different synthetic $\delta^{15}\text{N}$ time series were created from eight known temperature histories. The fitting approach leads to an excellent agreement in timing and amplitudes between the modelled and synthetic $\delta^{15}\text{N}$ and temperature data, ~~leading to mismatches in the low permeg level for $\delta^{15}\text{N}$ and to related temperature deviations of a few tenths of Kelvin (2σ , respectively).~~ The obtained, final mismatches follow a symmetric, standard distribution function. 95% of the mismatches compared to the synthetic data are in an envelope in between 3.0-~~permeg to 6.3-permeg~~ for $\delta^{15}\text{N}$ and 0.23-~~K to 0.51-K for K for temperature, depending on the synthetic temperature- history scenarios~~. These values can therefore be used as a 2σ estimate for the reconstruction uncertainty ~~arising from the presented fitting algorithm itself~~. For $\delta^{15}\text{N}$ the obtained final uncertainties are in the same order of magnitude as state of the art experimental measurement uncertainty. The presented reconstruction approach was also successfully applied to $\delta^{40}\text{Ar}$ and $\delta^{15}\text{N}_{\text{excess}}$ ~~measured data (Döring et al., in prep.). After the successful tests of the presented method using synthetic data, it is worthwhile to apply it in a next step to existing high resolution isotope measurements. Besides Holocene temperature reconstructions, Moreover, we have shown that~~ the presented fitting approach can also be applied to glacial temperature reconstructions (Döring et al., in prep.), ~~and it is with minor algorithm modifications. Based on the demonstrated flexibility of our inversion methodology, it is~~ reasonable to adapt ~~the~~ this approach for reconstructions of other non-linear physical processes.

Competing interests

The authors declare that they have no competing financial interests.

Acknowledgements

This work was supported by the SNF grants (SNF-159563 and SNF-172550). We would like to thank Drs. Takuro Kobashi, Philippe Kindler and Myriam Guillevic for helpful discussions about the ice core data and model ~~shortcomings/peculiarities~~.

References

- 5 [NGRIP members: Andersen, K. K., Azuma, N., Barnola, J.-M., Bigler, M., Biscaye, P., Caillon, N., Chappellaz, J., Clausen, H. B., Dahl-Jensen, D., Fischer, H., Flückiger, J., Fritzsche, D., Fujii, Y., Goto-Azuma, K., Grønbold, K., Gundestrup, N. S., Hansson, M., Huber, C., Hvidberg, C. S., Johnsen, S. J., Jonsell, U., Jouzel, J., Kipfstuhl, S., Landais, A., Leuenberger, M., Lorrain, R., Masson-Delmotte, V., Miller, H., Motoyama, H., Narita, H., Popp, T., Rasmussen, S. O., Raynaud, D., Rothlisberger, R., Ruth, U., Samyn, D., Schwander, J., Shoji, H., Siggard-Andersen, M.-L., Steffensen, J. P., Stocker, T., Sveinbjörnsdóttir, A. E., Svensson, A., Takata, M., Tison, J.-L., Thorsteinsson, T., Watanabe, O., Wilhelms, F. and White, J. W. C.: High-resolution record of Northern Hemisphere climate extending into the last interglacial period. *Nature*, 431\(7005\), 147–151. doi:10.1038/nature02805, 2004.](#)
- 10 Barnola, J.-M., Pimienta, P., Raynaud, D. and Korotkevich, Y. S.: CO₂-climate relationship as deduced from the Vostok ice core: a re-examination based on new measurements and on a re-evaluation of the air dating, *Tellus B*, 43(2), 83–90, doi:10.1034/j.1600-0889.1991.t01-1-00002.x, 1991.
- Beaulieu, J. L. de, Brugiapaglia, E., Joannin, S., Guiter, F., Zanchetta, G., Wulf, S., Peyron, O., Bernardo, L., Didier, J., Stock, A., Rius, D. and Magny, M.: Lateglacial-Holocene abrupt vegetation changes at Lago Trifoglietti in Calabria, Southern Italy: The setting of ecosystems in a refugial zone, *Quat. Sci. Rev.*, 158, 44–57, doi:10.1016/j.quascirev.2016.12.013, 2017.
- 15 Boersma-Klein, V. and De Vries, A. E.: The influence of the distribution of atomic masses within the molecule on thermal diffusion, *Physica*, 32, 717–733, doi:10.1016/0031-8914(66)90004-8, 1966.
- Box, G. E. P., Jenkins, G. M. and Reinsel, G. C.: *Time Series Analysis - Forecasting and Control*, 1994.
- 20 [Capron, E., Landais, A., Chappellaz, J., Schilt, A., Buiron, D., Dahl-Jensen, D., Johnsen, S. J., Jouzel, J., Lemieux-Dudon, B., Loulergue, L., Leuenberger, M., Masson-Delmotte, V., Mayer, H., Oerter, H. and Stenni, B.: Millennial and sub-millennial scale climatic variations recorded in polar ice cores over the last glacial period, *Clim. Past Discuss.*, 6\(1\), 135–183. doi:10.5194/cpd-6-135-2010, 2010.](#)
- Craig, H., Horibe, Y. and Sowers, T.: Gravitational separation of gases and isotopes in polar ice caps., *Science* (80-.), 242(4886), 1675–8, doi:10.1126/science.242.4886.1675, 1988.
- 25 Crank, J.: *The Mathematics of Diffusion*, 414 pp., Clarendon, —, [\[online\] Available from: https://scholar.google.ch/scholar?q=Crank%2C+J.+The+Mathematics+of+Diffusion%2C+414pp.%2C+Clarendon%2C+Oxford%2C+England%2C+%281975%29.&btnG=&hl=de&as_sdt=0%2C5](https://scholar.google.ch/scholar?q=Crank%2C+J.+The+Mathematics+of+Diffusion%2C+414pp.%2C+Clarendon%2C+Oxford%2C+England%2C+%281975%29.&btnG=&hl=de&as_sdt=0%2C5) (Accessed 21 March 2017), 1975.
- 30 Crausbay, S. D., Higuera, P. E., Sprugel, D. G. and Brubaker, L. B.: Fire catalyzed rapid ecological change in lowland coniferous forests of the Pacific Northwest over the past 14,000 years, *Ecology*, doi:10.1002/ecy.1897, 2017.
- Cuffey, K. M. and Clow, G. D.: Temperature, accumulation, and ice sheet elevation in central Greenland through the last deglacial transition, *J. Geophys. Res. Ocean.*, 102(C12), 26383–26396, doi:10.1029/96JC03981, 1997.

- Cuffey, K. M., Clow, G. D., Alley, R. B., Stuiver, M., Waddington, E. D. and Saltus, R. W.: Large Arctic Temperature Change at the Wisconsin-Holocene Glacial Transition. *Science*, 270(5235), 455–458, doi:10.1126/science.270.5235.455, 1995.
- Dahl-Jensen, D., Mosegaard, K., Gundestrup, N., Clow, G. D., Johnsen, S. J., Hansen, A. W. and Balling, N.: Past Temperatures Directly from the Greenland Ice Sheet, *Science* (80-.), 282(5387), 268–271, doi:10.1126/science.282.5387.268, 1998.
- Dansgaard, W., Clausen, H. B., Gundestrup, N., Hammer, C. U., Johnsen, S. F., Kristinsdottir, P. M. and Reeh, N.: A new greenland deep ice core., *Science*, 218(4579), 1273–7, doi:10.1126/science.218.4579.1273, 1982.
- Denton, G. H. and Karle'n, W.: Holocene climatic variations: their pattern and possible cause., *Quat. Res.*, 3(2), 155–205, doi:10.1016/0033-5894(73)90040-9, 1973.
- Enting, I. G.: On the Use of Smoothing Splines to Filter CO₂ Data, *J. Geophys. Res.*, 92(D9), 10977–10984, doi:10.1029/JD092iD09p10977, 1987.
- Etheridge, D. M., Pearman, G. I. and Fraser, P. J.: Changes in tropospheric methane between 1841 and 1978 from a high accumulation-rate Antarctic ice core, *Tellus B*, 44(4), 282–294, doi:10.1034/j.1600-0889.1992.t01-3-00006.x, 1992.
- Fourteau, K., Faïn, X., Martinerie, P., Landais, A., Ekaykin, A. A., Lipenkov, V. Y. and Chappellaz, J.: Analytical constraints on layered gas trapping and smoothing of atmospheric variability in ice under low accumulation conditions, *Clim. Past Discuss.*, 1–28, doi:10.5194/cp-2017-78, 2017.
- Fujita, S., Okuyama, J., Hori, A. and Hondoh, T.: Metamorphism of stratified firn at Dome Fuji, Antarctica: A mechanism for local insolation modulation of gas transport conditions during bubble close off, *J. Geophys. Res. Solid Earth*, 114(3), doi:10.1029/2008JF001143, 2009.
- Goujon, C., Barnola, J.-M. and Ritz, C.: Modeling the densification of polar firn including heat diffusion: Application to close-off characteristics and gas isotopic fractionation for Antarctica and Greenland sites, *J. Geophys. Res. Atmos.*, 108(D24), n/a-n/a, doi:10.1029/2002JD003319, 2003.
- Grachev, A. M. and Severinghaus, J. P.: Laboratory determination of thermal diffusion constants for 29N₂/28N₂ in air at temperatures from -60 to 0°C for reconstruction of magnitudes of abrupt climate changes using the ice core fossil-air plaeothermometer, *Geochim. Cosmochim. Acta*, 67(3), 345–360, doi:10.1016/S0016-7037(02)01115-8, 2003.
- Grachev, A. M. and Severinghaus, J. P.: A revised + 10±4°C magnitude of the abrupt change in Greenland temperature at the Younger Dryas termination using published GISP2 gas isotope data and air thermal diffusion constants, *Quat. Sci. Rev.*, 24(5–6), 513–519, doi:10.1016/j.quascirev.2004.10.016, 2005.
- Grootes, P. M. and Stuiver, M.: Oxygen 18/16 variability in Greenland snow and ice with 10-3- to 105-year time resolution, *J. Geophys. Res. Ocean.*, 102(C12), 26455–26470, doi:10.1029/97JC00880, 1997.
- Grootes, P. M., Stuiver, M., White, J. W. C., Johnsen, S. and Jouzel, J.: Comparison of oxygen isotope records from the GISP2 and GRIP Greenland ice cores, *Nature*, 366(6455), 552–554, doi:10.1038/366552a0, 1993.
- Guillevic, M.: PhD thesis., 2013.

- Guillevic, M., Bazin, L., Landais, A., Kindler, P., Orsi, A., Masson-Delmotte, V., Blunier, T., Buchardt, S. L., Capron, E.,
Leuenberger, M., Martinerie, P., Prié, F. and Vinther, B. M.: Spatial gradients of temperature, accumulation and
 $\delta^{18}\text{O}$ - ice in Greenland over a series of Dansgaard-Oeschger events, *Clim. Past*, 9(3), 1029–1051, doi:10.5194/cp-
9-1029-2013, 2013.
- 5 | Hedges L. V., O. I.: Statistical methods for meta-analysis. Academic Press, San Diego., 1985.
- Herron, M. M. and Langway, C. C.: Firm densification: an empirical model., *J. Glaciol.*, 25(93), 373–385,
doi:10.1017/S0022143000015239, 1980.
- Holmgren, K., Gogou, A., Izdebski, A., Luterbacher, J., Sicre, M. A. and Xoplaki, E.: Mediterranean Holocene climate,
environment and human societies, *Quat. Sci. Rev.*, 136, 1–4, doi:10.1016/j.quascirev.2015.12.014, 2016.
- 10 | Hörhold, M. W., Kipfstuhl, S., Wilhelms, F., Freitag, J. and Frenzel, A.: The densification of layered polar firm, *J. Geophys.*
Res. Earth Surf., 116(1), doi:10.1029/2009JF001630, 2011.
- Huber, C. and Leuenberger, M.: Measurements of isotope and elemental ratios of air from polar ice with a new on-line
extraction method, *Geochemistry, Geophys. Geosystems*, 5(10), n/a-n/a, doi:10.1029/2004GC000766, 2004.
- Huber, C., Leuenberger, M., Spahni, R., Flückiger, J., Schwander, J., Stocker, T. F., Johnsen, S., Landais, A. and Jouzel, J.:
15 | Isotope calibrated Greenland temperature record over Marine Isotope Stage 3 and its relation to CH₄, *Earth Planet.*
Sci. Lett., 243(3–4), 504–519, doi:10.1016/j.epsl.2006.01.002, 2006.
- Johnsen, S. J., Clausen, H. B., Dansgaard, W., Fuhrer, K., Gundestrup, N., Hammer, C. U., Iversen, P., Jouzel, J., Stauffer,
B. and Steffensen, J. P.: Irregular glacial interstadials recorded in a new Greenland ice core, *Nature*, 359(6393),
311–313, doi:10.1038/359311a0, 1992.
- 20 | Johnsen, S. J., Dahl-Jensen, D., Gundestrup, N., Steffensen, J. P., Clausen, H. B., Miller, H., Masson-Delmotte, V.,
Sveinbjörnsdóttir, A. E. and White, J.: Oxygen isotope and palaeotemperature records from six Greenland ice-core
stations: Camp Century, Dye-3, GRIP, GISP2, Renland and NorthGRIP, *J. Quat. Sci.*, 16(4), 299–307,
doi:10.1002/jqs.622, 2001.
- 25 | Kawamura, K., Severinghaus, J. P., Ishidoya, S., Sugawara, S., Hashida, G., Motoyama, H., Fujii, Y., Aoki, S. and
Nakazawa, T.: Convective mixing of air in firm at four polar sites, *Earth Planet. Sci. Lett.*, 244(3–4), 672–682,
doi:10.1016/j.epsl.2006.02.017, 2006.
- Kawamura, K., Severinghaus, J. P., Albert, M. R., Courville, Z. R., Fahnestock, M. A., Scambos, T., Shields, E. and
Shuman, C. A.: Kinetic fractionation of gases by deep air convection in polar firm, *Atmos. Chem. Phys.*, 13(21),
11141–11155, doi:10.5194/acp-13-11141-2013, 2013.
- 30 | Kindler, P., Guillevic, M., Baumgartner, M., Schwander, J., Landais, A. and Leuenberger, M.: Temperature reconstruction
from 10 to 120 kyr b2k from the NGRIP ice core, *Clim. Past*, 10(2), 887–902, doi:10.5194/cp-10-887-2014, 2014.
- Kobashi, T., Severinghaus, J. P. and Barnola, J. M.: 4 ± 1.5 °C abrupt warming 11,270 yr ago identified from trapped air in
Greenland ice, *Earth Planet. Sci. Lett.*, 268(3–4), 397–407, doi:10.1016/j.epsl.2008.01.032, 2008a.

- [Kobashi, T., Severinghaus, J. P. and Kawamura, K.: Argon and nitrogen isotopes of trapped air in the GISP2 ice core during the Holocene epoch \(0-11,500 B.P.\): Methodology and implications for gas loss processes, *Geochim. Cosmochim. Acta*, 72\(19\), 4675–4686, doi:10.1016/j.gca.2008.07.006, ~~2008~~2008b.](#)
- Kobashi, T., Kawamura, K., Severinghaus, J. P., Barnola, J. M., Nakaegawa, T., Vinther, B. M., Johnsen, S. J. and Box, J. E.: High variability of Greenland surface temperature over the past 4000 years estimated from trapped air in an ice core, *Geophys. Res. Lett.*, 38(21), n/a-n/a, doi:10.1029/2011GL049444, 2011.
- [Kobashi, T., Menviel, L., Jeltsch-Thömmes, A., Vinther, B. M., Box, J. E., Muscheler, R., Nakaegawa, T., Pfister, P. L., Döring, M., Leuenberger, M., Wanner, H. and Ohmura, A.: Volcanic influence on centennial to millennial Holocene Greenland temperature change, *Sci. Rep.*, 7\(1\), 1441, doi:10.1038/s41598-017-01451-7, 2017.](#)
- [Landais, A., Barnola, J. M., Masson-Delmotte, V., Jouzel, J., Chappellaz, J., Caillon, N., Huber, C., Leuenberger, M. and Johnsen, S. J.: A continuous record of temperature evolution over a sequence of Dansgaard-Oeschger events during Marine Isotopic Stage 4 \(76 to 62 kyr BP\), *Geophys. Res. Lett.*, 31\(22\), 1–4, doi:10.1029/2004GL021193, 2004.](#)
- Lespez, L. et al.: Rapid climatic change and social transformations Uncertainties, adaptability and resilience, in *The Mediterranean Region under Climate Change A Scientific Update*, p. 738, Marseille., 2016.
- Leuenberger, M. C., Lang, C. and Schwander, J.: $\delta^{15}\text{N}$ measurements as a calibration tool for the paleothermometer and gas-ice age differences: A case study for the 8200BP event on GRIP ice, *J. Geophys. Res.*, 104(D18), 22163–22170, doi:10.1029/1999jd900436, 1999.
- Mariotti, A.: Atmospheric nitrogen is a reliable standard for natural ^{15}N abundance measurements, *Nature*, 303(5919), 685–687, doi:10.1038/303685a0, 1983.
- Martinerie, P., Lipenkov, V. Y., Raynaud, D., Chappellaz, J., Barkov, N. I. and Lorius, C.: Air content paleo record in the Vostok ice core (Antarctica): A mixed record of climatic and glaciological parameters, *J. Geophys. Res.*, 99(D5), 10565, doi:10.1029/93JD03223, 1994.
- [Masson-Delmotte, V.: GRIP Deuterium Excess Reveals Rapid and Orbital-Scale Changes in Greenland Moisture Origin, *Science* \(80-. \), 309\(5731\), 118–121, doi:10.1126/science.1108575, 2005.](#)
- Mayewski, P., Rohling, E., Curt Stager, J., Karlén, W., Maasch, K. A., David Meeker, L., Meyerson, E. A., Gasse, F., van Kreveld, S., Holmgren, K., Lee-Thorp, J., Rosqvist, G., Rack, F., Staubwasser, M., Schneider, R. and Steig, E. J.: Holocene climate variability, *Quat. Res.*, 62(3), 243–255, doi:10.1016/j.yqres.2004.07.001, 2004.
- Meese, D. A., Alley, R. B., Flacco, R. J., Germani, M. S., Gow, A. J., Grootes, P. M., Illing, M., Mayewski, P. A., Morrison, M. C., Ram, M., Taylor, K., Yang, Q. and Zielinski, G. A.: Preliminary depth-age scale of the GISP2 ice core, 1994.
- [Orsi, A. J., Cornuelle, B. D. and Severinghaus, J. P.: Magnitude and temporal evolution of Dansgaard-Oeschger event 8 abrupt temperature change inferred from nitrogen and argon isotopes in GISP2 ice using a new least-squares inversion, *Earth Planet. Sci. Lett.*, 395, 81–90, doi:10.1016/j.epsl.2014.03.030, 2014.](#)

Pál, I., Buczkó, K., Vincze, I., Finsinger, W., Braun, M., Biró, T. and Magyari, E. K.: Terrestrial and aquatic ecosystem responses to early Holocene rapid climate change (RCC) events in the South Carpathian Mountains, Romania, *Quat. Int.*, doi:10.1016/j.quaint.2016.11.015, 2016.

Rasmussen, S. O., Seierstad, I. K., Andersen, K. K., Bigler, M., Dahl-Jensen, D. and Johnsen, S. J.: Synchronization of the NGRIP, GRIP, and GISP2 ice cores across MIS 2 and palaeoclimatic implications, *Quat. Sci. Rev.*, 27(1–2), 18–28, doi:10.1016/j.quascirev.2007.01.016, 2008.

Rasmussen, S. O., Bigler, M., Blockley, S. P., Blunier, T., Buchardt, S. L., Clausen, H. B., Cvijanovic, I., Dahl-Jensen, D., Johnsen, S. J., Fischer, H., Gkinis, V., Guillevic, M., Hoek, W. Z., Lowe, J. J., Pedro, J. B., Popp, T., Seierstad, I. K., Steffensen, J. P., Svensson, A. M., Vallelonga, P., Vinther, B. M., Walker, M. J. C., Wheatley, J. J. and Winstrup, M.: A stratigraphic framework for abrupt climatic changes during the Last Glacial period based on three synchronized unchronized Greenland ice-core records: Refining and extending the INTIMATE event stratigraphy, *Quat. Sci. Rev.*, 106, 14–28, doi:10.1016/j.quascirev.2014.09.007, 2014.

Rhodes, R. H., Faïn, X., Stowasser, C., Blunier, T., Chappellaz, J., McConnell, J. R., Romanini, D., Mitchell, L. E. and Brook, E. J.: Continuous methane measurements from a late Holocene Greenland ice core: Atmospheric and in-situ signals, *Earth Planet. Sci. Lett.*, 368, 9–19, doi:10.1016/j.epsl.2013.02.034, 2013.

Rhodes, R. H., Faïn, X., Brook, E. J., McConnell, J. R., Maselli, O. J., Sigl, M., Edwards, J., Buizert, C., Blunier, T., Chappellaz, J. and Freitag, J.: Local artifacts in ice core methane records caused by layered bubble trapping and in situ production: A multi-site investigation, *Clim. Past*, 12(4), 1061–1077, doi:10.5194/cp-12-1061-2016, 2016.

Rosen, J. L., Brook, E. J., Severinghaus, J. P., Blunier, T., Mitchell, L. E., Lee, J. E., Edwards, J. S. and Gkinis, V.: An ice core record of near-synchronous global climate changes at the Bølling transition, *Nat. Geosci.*, 7(6), 459–463, doi:10.1038/ngeo2147, 2014.

Schwander, J.: The Transformation of Snow to Ice and the Occlusion of Gases, in *The Environmental Record in Glaciers and Ice Sheets*, pp. 53–67., 1989.

Schwander, J., Barnola, J.-M., Andrié, C., Leuenberger, M., Ludin, A., Raynaud, D. and Stauffer, B.: The age of the air in the firn and the ice at Summit, Greenland, *J. Geophys. Res.*, 98(D2), 2831–2838, doi:10.1029/92JD02383, 1993.

Schwander, J., Sowers, T., Barnola, J. M., Blunier, T., Fuchs, A. and Malaizé, B.: Age scale of the air in the summit ice: —Implication for glacial-interglacial temperature change, *J. Geophys. Res.*, 102(D16), 19483–19493, doi:10.1029/97JD01309, 1997.

Seierstad, I. K., Abbott, P. M., Bigler, M., Blunier, T., Bourne, A. J., Brook, E., Buchardt, S. L., Buizert, C., Clausen, H. B., Cook, E., Dahl-Jensen, D., Davies, S. M., Guillevic, M., Johnsen, S. J., Pedersen, D. S., Popp, T. J., Rasmussen, S. O., Severinghaus, J. P., Svensson, A. and Vinther, B. M.: Consistently dated records from the Greenland GRIP, GISP2 and NGRIP ice cores for the past 104ka reveal regional millennial-scale d18O gradients with possible Heinrich event imprint, *Quat. Sci. Rev.*, 106, 29–46, doi:10.1016/j.quascirev.2014.10.032, 2014.

- Severinghaus, J. P., Sowerst, T. and Alley, R. B.: Timing of abrupt climate change at the end of the Younger Dryas interval -from thermally fractionated gases in polar ice, *Nature*, 39(January), 141–146, doi:10.1002/jqs.622, 1998.
- Severinghaus, J. P., Grachev, A. and Battle, M.: Thermal fractionation of air in polar firn by seasonal temperature gradients, *Geochemistry, Geophys. Geosystems*, 2(7), n/a-n/a, doi:10.1029/2000GC000146, 2001.
- 5 [Severinghaus, J. P., Albert, M. R., Courville, Z. R., Fahnestock, M. A., Kawamura, K., Montzka, S. A., Mühle, J., Scambos, T. A., Shields, E., Shuman, C. A., Suwa, M., Tans, P. and Weiss, R. F.: Deep air convection in the firn at a zero-accumulation site, central Antarctica, *Earth Planet. Sci. Lett.*, 293\(3–4\), 359–367, doi:10.1016/j.epsl.2010.03.003, 2010.](#)
- 10 [Spahni, R.: The attenuation of fast atmospheric CH₄ variations recorded in polar ice cores, *Geophys. Res. Lett.*, 30\(11\), 1571, doi:10.1029/2003GL017093, 2003.](#)
- Steig, E. J., Grootes, P. M. and Stuiver, M.: Seasonal Precipitation Timing and Ice Core Records, *Science* (80-.), 266(5192), 1885–1886, doi:10.1126/science.266.5192.1885, 1994.
- Stuiver, M., Grootes, P. M. and Braziunas, T. F.: The GISP2 ~~41805180~~ Climate Record of the Past 16,500 Years and the Role of the Sun, Ocean, and Volcanoes, *Quat. Res.*, 44(3), 341–354, doi:10.1006/qres.1995.1079, 1995.
- 15 Werner, M., Heimann, M. and Hoffmann, G.: Isotopic composition and origin of polar precipitation in present and glacial climate simulations, *Tellus Ser. B Chem. Phys. Meteorol. B*, 53, doi:10.1034/j.1600-0889.2001.01154.x, 2001.